Case Studies in Thermal Engineering 81 (2026) 108000

Contents lists available at ScienceDirect

Case Studies in Thermal Engineering

journal homepage: www.elsevier.com/locate/csite

Experimental investigation on thermal and moisture performance of direct evaporative cooling coupled with phase change plates for data centers

Yangyang Zhang [a], Hongli Xu [a], Jiri Zhou [b], Xing Liang [c], Hongwei Wu [d], Ruiyong Mao [a], Zujing Zhang [a,*]

[a] College of Civil Engineering, State Key Laboratory of Public Big Data, Guizhou University, Guiyang 550025, China
[b] China MCC5 Group CORP.LTD., MCC5 Tower, No. 9 Wuye Road, Jinjiang District, Chengdu, 610000, China
[c] School of Computer Science and Mathematics, Kingston University London, KT1 2EE, United Kingdom
[d] School of Physic, Engineering and Computer Science, University of Hertfordshire, Hatfield, AL10 9AB, United Kingdom

GRAPHICAL ABSTRACT

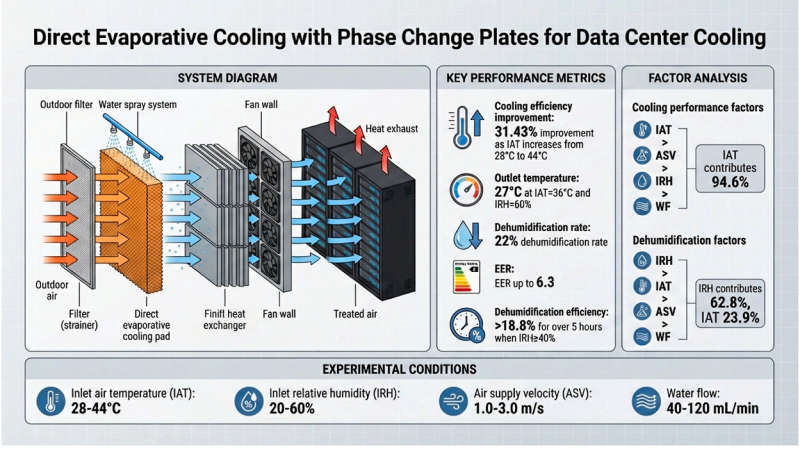

ARTICLE INFO

Keywords:
Phase change energy storage

ABSTRACT

Direct evaporative cooling is widely used in data centers but risks elevating humidity. This study proposes a direct ventilation channel system integrating direct evaporative cooling with phase

* Corresponding author.
E-mail address: zjzhang3@gzu.edu.cn (Z. Zhang).

https://doi.org/10.1016/j.csite.2026.108000
Received 16 December 2025; Received in revised form 18 February 2026; Accepted 28 March 2026
Available online 30 March 2026

Free cooling
Direct evaporative cooling
Data center
Cooling
Dehumidification

change plates. Experiments investigated effects of inlet air temperature (IAT: 28–44 °C), inlet relative humidity (IRH: 20–60%), air supply velocity (ASV: 1.0–3.0 m/s), and water flow (40–120 mL/min). Results show: (I) The coupled system exhibits synergistic effects, achieving 31.43% cooling efficiency improvement as IAT increases from 28 °C to 44 °C. (II) At IAT = 36 °C and IRH = 60%, outlet temperature reaches 27 °C with 62.3% RH, achieving 22% dehumidification rate. Dehumidification efficiency exceeds 18.8% for over 5 h when IRH≥40%. (III) Cooling performance factors order: IAT > ASV > IRH > WF, with IAT contributing 94.6%. Dehumidification factors order: IRH > IAT > ASV > WF, with IRH contributing 62.8% and IAT 23.9%. The system achieves EER up to 6.3 when meeting data center cooling demand (1728–3456 m^3/h) at 30–32 °C. This study provides a feasible energy-saving cooling strategy for data centers.

Nomenclature

Greek symbols		Abbreviation	
T_{in}	Inlet air temperature, °C	PCES	Phase Change Energy Storage
RH_{in}	Inlet air relative humidity, %	PCM	Phase Change Materials
T_{out}	Outlet air temperature, °C	PCP	Phase Change Plates
RH_{out}	Outlet air relative humidity, %	DEC	Direct evaporative cooling
v_a	Air supply velocity, m/s	DVC	Direct ventilation channel
v_w	Water flow, ml/min	SDEC	Spraying direct evaporative cooling
σ_Y	Uncertainty	DPDEC	Drip padding direct evaporative cooling
ΔT	Temperature difference, °C	IAT	Inlet air temperature
ΔT_1	ΔT between the inlet and outlet, °C	IRH	Inlet air relative humidity
ΔT_2	ΔT between the front and rear ends of direct evaporative cooling, °C	ASV	Air supply velocity
ΔT_3	ΔT between the front and rear ends of PCP, °C	WF	Water flow
d	Humidity ratio, g/kg	EER	Energy efficiency ratio
Δd_1	The amount of dehumidification of the system, g/kg		
Δd_2	The amount of humidification of DEC, g/kg		
Δd_3	The amount of dehumidification of PCP, g/kg		

1. Introduction

With the rapid development of technologies such as cloud computing, big data, and AI [1–3], the scale and number of data centers are growing [4]. In today's information age, the energy consumption of data centers has been one of the focuses of attention [5–7], and their energy demand is also increasing [8]. According to statistics, the power consumed by data centers around the world has accounted for a considerable proportion of global electricity consumption [9], which is still growing [10]. The energy consumption of cooling systems occupies about 40% of the data center's cooling total energy [11,12], and the large energy consumption of cooling is more prominent in the summer [13]. To reduce the cooling energy consumption in data centers, cooling technologies need to be innovatively optimized [14].

Free cooling sends fresh air into the server room to cool it down [15], effectively reducing the energy consumption of the cooling systems [16]. Zhang et al. [17] analyzed and compared four types of natural cooling systems for data centers and found that direct fresh-air cooling has a high potential and a high energy-saving rate. Zhou et al. [18] proposed an optimization method of direct air natural cooling for data center, which could save up to 5% of the total energy in the summer. Yu et al. [19] designed a solid adsorption heat pipe coupled with direct air natural cooling technology for data center rack-level thermal control, which could reduce the peak server temperature from 75.8 °C to 68.8 °C. In practical operation, the work of a server room usually needs to run 24 h a day [20]. However, natural cooling sources do not always provide sufficient cooling even in areas where temperatures are usually low [21].

However, direct evaporative cooling (DEC) can provide sufficient and stable cold sources for data centers. DEC is an energy-efficient, low-carbon, and cost-effective refrigeration technology [22,23]. Al-Badri et al. [24] found that using cold water and reducing the mass flow rate ratio significantly improves the DEC performance when the air humidity is high. Li et al. [25] used a cold mist evaporative cooling technique to cool the fresh air, which showed that the treated air reached the air supply requirements of the data center when the RH was lower than 40%. More studies on DEC have found that DEC can be used in low-humidity areas to humidify cool and filter the outdoor fresh air [26], and in medium and high-humidity areas it can be used for pre-cooling and energy recovery of fresh air [27,28]. Although DEC technology provides effective cooling for data centers, the issue of excessive humidity still exists, causing the over relative humidity in data center. Additionally, DEC increases water demand, posing challenges in arid or water-stressed regions [29].

Natural cold sources can be stored with the help of phase change energy storage (PCES). PCES utilizes the property of phase change material (PCM) to release or absorb latent heat during temperature change to store or release energy [30,31], which has the advantages of high energy storage density [32] and environmental friendliness [33]. Zhu et al. [34] proposed a finned tube combined with the PCM heat exchanger for data center cooling, achieving the highest average heat exchange capacity rate when melted to 50% of its total capacity. Ma et al. [35] proposed a cooling system consisting of water-loaded annular thermosiphon tubes and paraffin-loaded polytubes, which demonstrated that servers could be maintained for 6 min during a power failure of the cooling system. Huang et al. [36] designed a PCM-based cooled storage unit for air-cooled modular data centers to maintain emergency cooling for 300s. Wang et al. [37] used composite PCM as a CPU coolant to achieve energy savings of 23%. Gao et al. [38] designed novel

experiments to elucidate the effect of high-humidity environments on the melting process of PCP, which showed that high-humidity environments increased the melting rate of PCP. For a system combining direct evaporative cooling and phase change cold storage. DEC provides efficient cooling, while PCM acts as a "cooling battery" to store excess cooling capacity. This combination significantly enhances the system's adaptability to high-humidity or high-load conditions, effectively reducing reliance on traditional mechanical refrigeration. It delivers comprehensive benefits, including energy savings, load shifting, and improved renewable energy utilization [39]. However, the system faces several challenges: PCM modules increase initial investment and occupy additional space, air-side heat exchange adds extra fan energy consumption, and complex control strategies are required to precisely coordinate the charging and discharging cycles. However, the working effect of PCM is susceptible to factors such as air temperature, relative humidity, and air velocity [40,41].

Based on the literature review, several research gaps are as follows. Firstly, DEC can effectively reduce air temperature, however, it tends to increase the relative humidity levels within the server room, thereby creating challenges in maintaining optimal conditions for sensitive equipment. Secondly, although free cooling and PCES provide significant energy savings for data center cooling, their performances are highly influenced by external climatic conditions. For example, they don't cool the air reliably and efficiently under high temperature, high humidity, or low wind speed conditions. Overall, these three cooling technologies have distinct advantages. However, they face challenges in consistently meeting the basic supply air temperature and RH standards for data centers in a stable and energy-efficient manner.

Therefore, this study integrated above technologies to develop a cooling and dehumidification system. The system not only processed and delivered air that reached the temperature and relative humidity standards for the data center, but also stably utilized renewable energy to reduce cooling energy consumption. An experimental platform was established based on the data center. Inlet air temperatures (IAT), inlet air relative humidity (IRH), air supply velocity (ASV), and water flow (WF) influence on system performance were investigated by a series of experimental studies under extreme summer conditions. Furthermore, orthogonal experiments were conducted to investigate the order of influence of these factors on the cooling and dehumidifying performance of the system. This study provided a feasible strategy for energy-efficient cooling in data centers.

2. Method

2.1. System principle

The highest temperatures recorded in the last five years in the cities represented by the eight arithmetic hub regions in China are compiled by the China Meteorological Network, see Fig. 1.

Fig. 2 shows the air temperature and humidity changes during the highest temperature in Guiyang, Guizhou Province, Chian, from 2023 to 2024. Guiyang has the highest recorded temperature reaching 34.3 °C. The corresponding relative humidity at high temperatures ranges from 32% to 83%. From 10:00 to 20:00, the temperature exceeds 27 °C, which does not meet the data center air supply standard [25]. The nighttime temperature is below the phase change temperature, which is conducive to PCM solidification. At night, natural cold air is utilized to cool the PCM for energy storage. During the day, air cooling is achieved by exchanging heat

Fig. 1. Data centers in the computing hub area represent cities with the highest dry bulb temperatures.

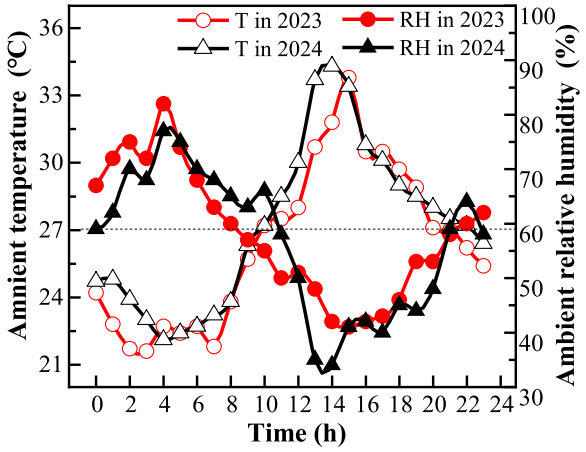

Fig. 2. Temperature and RH changes on the highest temperature day in Guiyang.

between the solidified PCM and the hot air.

The working schematic of the newly developed system is illustrated in Fig. 3. Outdoor high-temperature air is treated by the direct ventilation channel (DVC) designed in this study to meet the established standards. Then, it is directed to the racks to ensure the proper functioning of the servers. Initially, the air passes through the DEC section, which utilizes water evaporation to absorb heat, reducing its temperature. At this stage, the temperature is significantly reduced. However, the relative humidity may exceed the acceptable levels. Subsequently, following the evaporation and humidification of the air through the lower temperature of the PCP section once again for heat and humidity exchange. The air temperature is further lowered, along with a decrease in humidity ratio (*d*). Finally, the treated air is circulated through fans into the data center to cool the servers that are operating at elevated temperatures.

2.2. *Experimental principle*

Fig. 4 shows the basic principle of the experimental implementation process. The cooling room utilizes a refrigerator machine to circulate cold air into the DVC, simulating the natural nighttime climate. Therefore, the PCP can store the cold. When the PCM is completely solidified, the fresh air handling unit adjusts the outdoor air to the experimental conditions. Through the ventilation room, the air conditions during high summer temperatures are simulated.

Fig. 5 shows the structural composition of the system. The system mainly consists of DEC equipment, PCP, and air supply equipment. The DEC equipment plays an important role in the system and is mainly used to pre-cool and humidify the air. It has two roles. Firstly, it makes up for the shortcomings of phase change refrigeration alone and improves the cooling efficiency of the system. Secondly, favorable operating conditions are created for phase change dehumidification. The two types of DEC equipment are spray direct evaporative cooling (SDEC) and drip padding direct evaporative cooling (DPDEC). The SDEC produces cold air mainly relying on the high-pressure nozzles to atomize the water and then exchange heat and humidity with the air, as shown in Fig. 5 (a). In the DPDEC system, water is uniformly distributed onto the padding via a pump, forming a continuous water film on the surface of the padding. This configuration facilitates efficient heat and humidity exchange between the air and the water through the padding, as depicted in Fig. 5 (b). The PCPs are installed approximately 45 cm from the DEC unit to ensure air uniformity and eliminate the influence of water

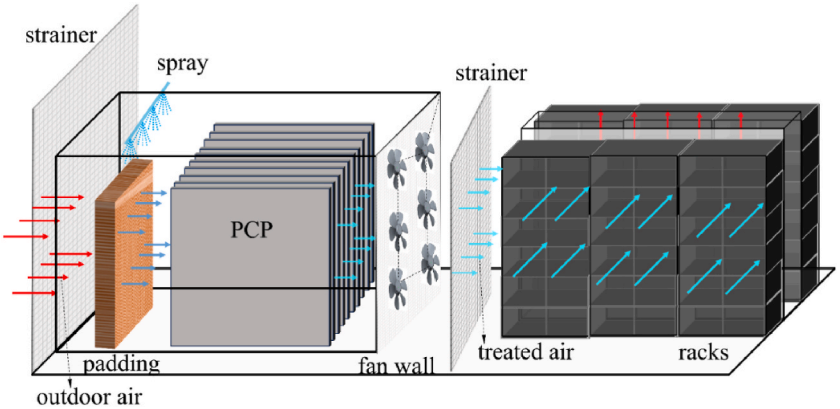

Fig. 3. Schematic of the system for data center cooling and dehumidification.

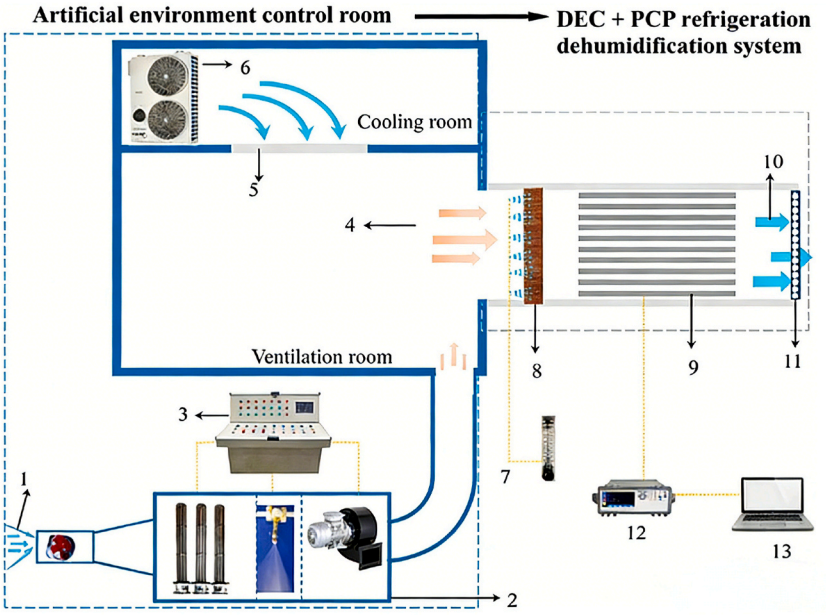

Fig. 4. Experimental principle.

vapor on temperature measurement. This distance allows the cool, moist airflow to fully mix and form a uniform temperature field, while preventing the sensors from being directly exposed to the high-humidity discharge, thereby obtaining accurate and reliable ambient temperature readings. PCP plays a key role in making this system feasible. At night, the natural cold air is stored using PCP solidification. During the daytime at high temperatures, the solidified PCP not only cools the evaporatively humidified and cooled air again but also dehumidifies it.

2.3. Experimental platform

The heat-moisture performance of the system was experimentally investigated in the civil engineering laboratory of Guizhou University. The experimental platform is shown in Fig. 6. The experimental platform mainly consists of two parts: the artificial environment room and the DVC system. Among them, the artificial environment room can control the air temperature in the environment laboratory at −20 °C~50 °C with a control accuracy of ≤±0.5 °C, and the RH at 20%~100% with a control accuracy of ≤±5 °C.

The dimension of the DVC was 200 cm (length) × 65 cm (width) × 65 cm (height), and its periphery was assembled by lapping 5 mm-thick acrylic panels, as shown in Fig. 7. The performance of this experiment was studied by having SDEC and DPDEC respectively coupled with PCP device of the type of DVC system. SDEC was realized through high-pressure nozzles. Six 8 mm caliber copper nozzles were placed from outside the channel by punching holes above the DVC. The nozzles were connected by a tee pipe with a spacing of 10 cm between each two nozzles. For DPDEC, an additional plant fiber padding was installed on top of the SDEC with a dimension of 65 cm (length) × 64 cm (height) × 10 cm (width). Both cooling devices were stabilized by a pump to deliver water with a temperature of 20 °C. A rotameter was connected to the pump outlet pipe to control the spray circulation v_w. The DEC device at the bottom of the channel has more tiny holes for drainage, the corresponding position of the bottom of the water tank placed below the water supply as well as collecting drainage.

The PCPs were systematically positioned 45 cm away from the DEC device. The charge and discharge detail of PCP is shown in Fig. 8. Turned off the spray at night, the cold air entered the gap between the PCPs so that the PCM solidified and the PCPs were charged. Turned on the spray by day, the high-temperature air entered the gap between the PCPs so that the PCM melted and the PCPs were discharged.

Each PCP was constructed from 1 mm thick tin-plated plates, with dimensions of 110 cm (length) × 3 cm (width) × 58 cm (height). The filler material used in the PCPs was paraffin. Its properties are shown in Table 1.

2.4. Data collection

A temperature and humidity detector was fixed in front of the channel entrance to monitor and adjust the T_{in} and RH_{in} in real-time. PT100 thermocouples with grade-A accuracy were used for temperature measurement. Four PT100 measurement points were arranged 30 cm away from the nozzle. The upper two measurement points were 22.5 cm away from the top of the channel, while the lower two were 20 cm away from the upper two measurement points. Two relative humidity measurement points were evenly

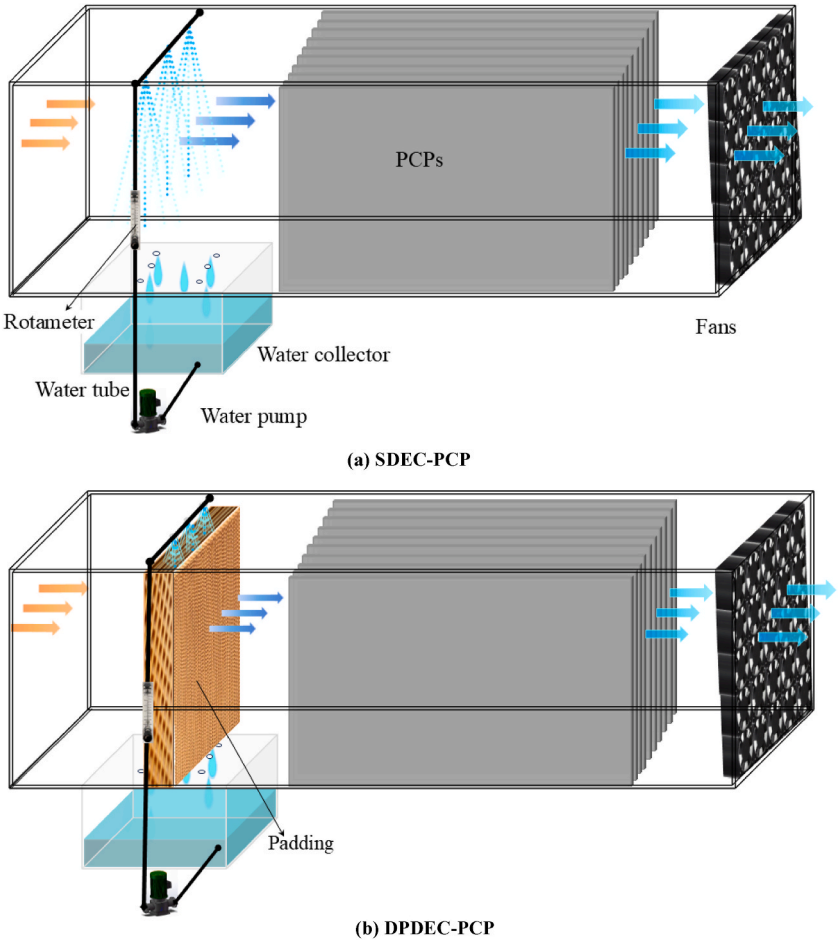

Fig. 5. Structure and schematic diagram of the combined system.

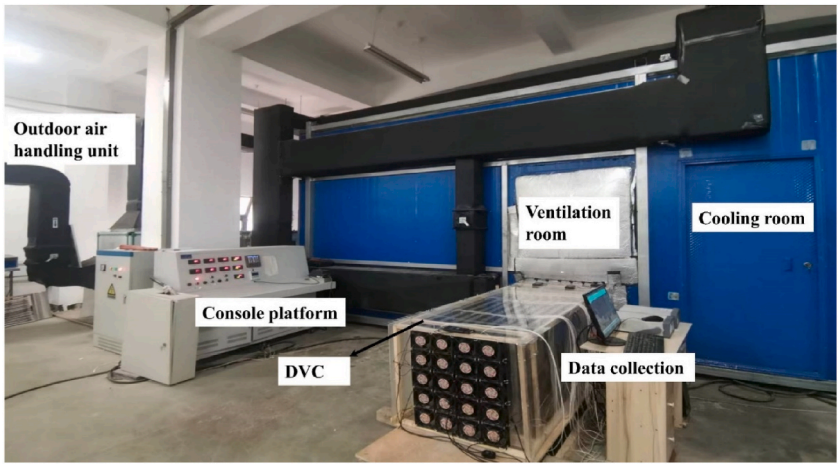

Fig. 6. Experimental platform diagram.

arranged between the upper and lower temperature measurement points. To grasp the temperature changes during the melting and solidification of the PCP, four PT100 measurement points were arranged inside each PCP. The measurement point at the exit was arranged in the middle of the back end of the PCP and the fan wall, and the arrangement was the same as measurement points after evaporative cooling, as shown in Fig. 9. During the experiment, an anemometer was used to measure and record every 5 min on the

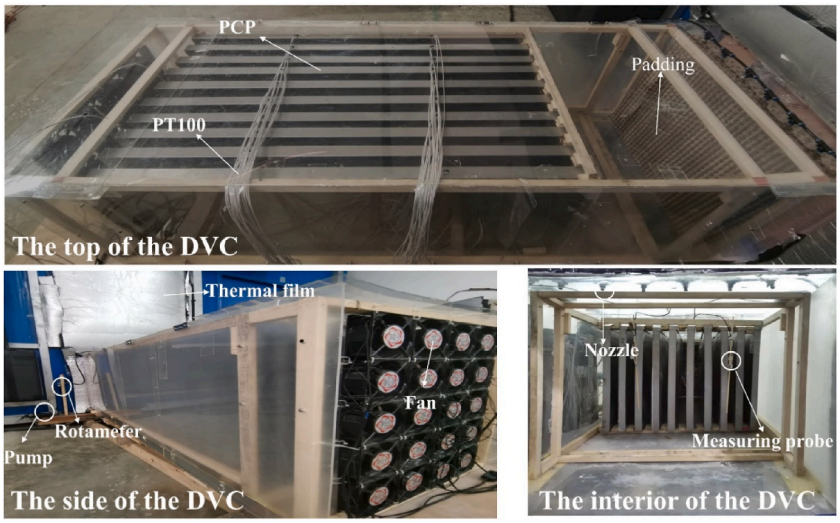

Fig. 7. Detailed view of the DVC.

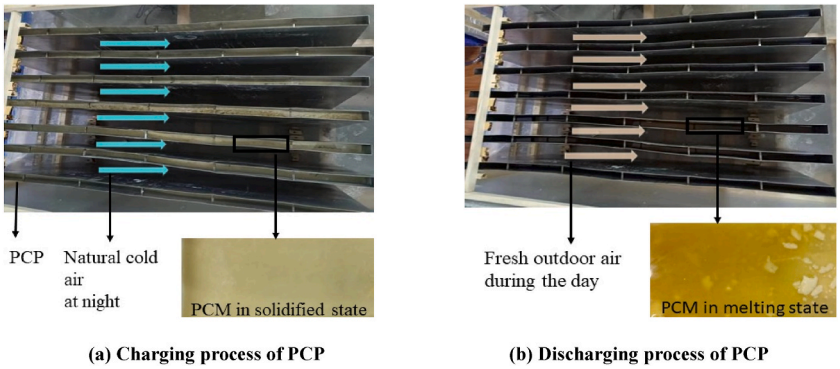

Fig. 8. Charge and discharge detail diagram of PCP.

Table 1
Properties of PCM.

Material	Paraffin
Phase change temperature range (°C)	21~25
Density (kg/m^3)	880
Thermal conductivity (W/(m·K))	0.21
Latent heat (kJ/kg)	217
Specific heat (kJ/(kg·°C))	3.22
Flashing point (°C)	>250
Maximum working point (°C)	200

outside of the fan wall at the exit of the ventilation channel.

There were 48 PT100 measurement points in the experiment. A total of two temperature data acquisition instruments were used, and the data recorded by the instruments were retained in one decimal place. Considering the long experimental period of 8 h, the measurement data were automatically recorded and stored once every 5 min for the sake of data integrity and credibility of the results. The main experimental equipment in the data acquisition process was unified before the start of the experiment was calibrated. Their models, specifications, and parameters are shown in Table 2.

2.5. Condition design

In this experiment, a controlled variable approach is used to conduct the experimental study. Firstly, the ability of PCP to cool in high temperature and high humidity environments is explored. Secondly, compared the cooling and dehumidification efficiency of two

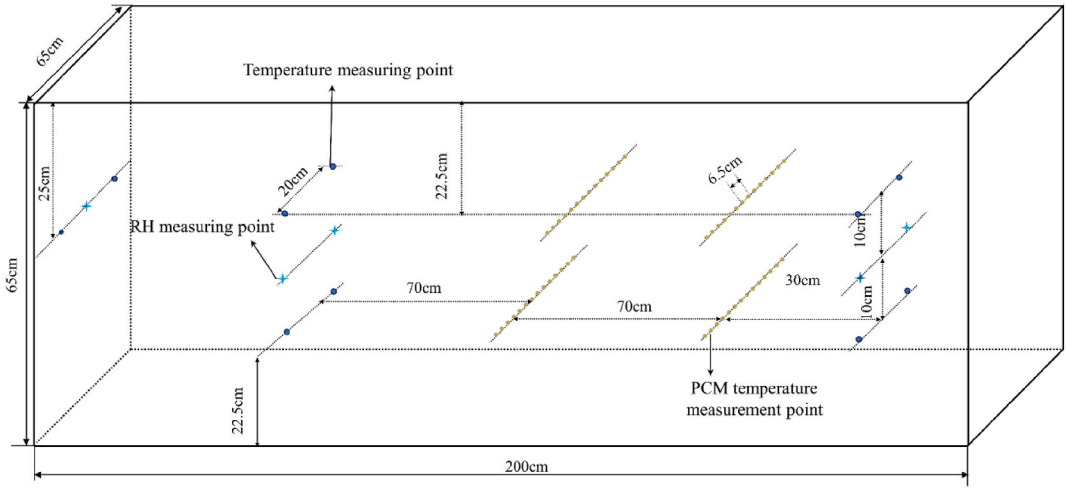

Fig. 9. Temperature and RH measurement point layout.

Table 2
Main equipment technical parameters table.

Instrument	Specification	Range	Accuracy
Temperature acquisition instrument	JK4032	−20 °C~70 °C	±(0.5% R-1)°C
RH acquisition instrument	ZL-TH10T	0%~99%	±3%
Rotameter	LZM-4T	40 ml/miñ200 ml/min	±0.02%
Anemometer	FLUKE-925	0.2 m/s ~20 m/s	±0.02%
Thermocouple	PT100	−50 °C~200 °C	Grade-A

DEC devices coupled with PCP to find a better system matching scheme. Finally, based on the conclusion of the previous step, the factors of T_{in}, RH_{in}, v_a, and vw on the performance of the system are investigated.

Data center stipulated that the fresh air volume should be the maximum of the following two: (1) 40 m^3/h per person based on the staff; (2) the air volume required to maintain the positive pressure in the room. As it is difficult to calculate the amount of fresh air required to maintain positive pressure in the room, according to experience and reference to the design of the clean room, the amount of fresh air can be calculated according to the number of air changes in the room 1-2 times/h. This experiment refers to the size of a data center server room in Guiyang to calculate the v_a of the DVC. The size of this server room is 18m (L) × 16m (W) × 6m (H). Its required air volume is 1728 m^3/h~3456 m^3/h, and the range of the v_a is 0.96 m/s~2.98 m/s. The v_a can be adjusted to 1.0 m/s, 1.5 m/s, 2.0 m/s, 2.5 m/s, and 3.0 m/s by the inverter. In summary, a total of 20 sets of experiments were designed, as shown in Table 3.

Table 3
Experimental condition.

Case	Device	T_{in} (°C)	RH_{in} (%)	v_a (m/s)	Vw (mL/min)
1	PCP	30	70	1.0	
2	SDEC- PCP	28	50	3.0	80
3	SDEC- PCP	32	50	3.0	80
4	DPDEC- PCP	28	50	3.0	80
5	DPDEC- PCP	32	50	3.0	80
6	DPDEC- PCP	36	50	3.0	80
7	DPDEC- PCP	40	50	3.0	80
8	DPDEC- PCP	44	50	3.0	80
9	DPDEC- PCP	36	60	3.0	80
10	DPDEC- PCP	36	40	3.0	80
11	DPDEC- PCP	36	30	3.0	80
12	DPDEC- PCP	36	20	3.0	80
13	DPDEC- PCP	36	50	2.5	80
14	DPDEC- PCP	36	50	2.0	80
15	DPDEC- PCP	36	50	1.5	80
16	DPDEC- PCP	36	50	1.0	80
17	DPDEC- PCP	36	50	2.0	120
18	DPDEC- PCP	36	50	2.0	100
19	DPDEC- PCP	36	50	2.0	60
20	DPDEC- PCP	36	50	2.0	40

2.6. Experimental procedure

During the experiment, the experimental parameters that need to be adjusted are T_{in}, RH_{in}, v_a, and v_w. Take case 4 for example, its main experimental steps are as follows:

(1) Place the sensor at each measurement point and open the calibrated temperature and humidity data acquisition instrument;
(2) On the artificial environment control platform to open the air-handling unit, open the control thermostatic air supply system, the T_{in} stabilized at 28 ± 0.5 °C, and the humidifier block to control the RH_{in} is 50 ± 2.5%;
(3) Control platform to open the fan and the channel exit at the axial fan, by adjusting the straight through the channel exit at the inverter control v_a of 3.0 ± 0.04 m/s;
(4) Turn on the water pump adjusting the rotameter to control the v_w of 80 ml/min;
(5) Maintain the aforementioned conditions throughout the full 8-h experiment, save the data, and then shut down the instrument.

2.7. Similarity analysis between the scaled model and the full-scale system

To validate whether the 2 m DVC test section can represent a full-scale air supply system, a similarity analysis based on dimensionless criteria was conducted. The full-scale prototype is a data center server room in Guiyang (18 m × 16 m × 6 m) with an air change rate (ACH) of 1–2 h^{-1}. The geometric scaling ratio between the model and prototype is approximately 1:9.

(1) Flow Similarity (Reynolds Number): The Reynolds numbers ($Re = \rho v D_h/\mu$) for both the model and prototype exceed 10^4 under typical operating conditions, indicating that the flow is in the turbulent self-similarity region. In this region, the flow field is independent of *Re*, allowing local resistance coefficients and heat/mass transfer efficiencies obtained from the model to be directly applied to the prototype.
(2) Thermal and Moisture Performance Similarity: The model accurately replicates the core functional components (DEC padding and PCPs) and their interaction with the airflow. Thus, dimensionless parameters such as cooling efficiency ($\Delta T_1/\ T_{in}$) and dehumidification efficiency ($\Delta d_3/d_{out}$) are directly transferable. The performance trends observed in the model represent the steady-state behavior of the full-scale system under similar inlet conditions.
(3) Temporal Scaling and Dynamic Response: The residence time of air in the model ($\tau_{model} = 2/v_a$, approximately 0.67–2 s) is much shorter than that in the full-scale room ($\tau_{prototype} = 1800$–$3600s$ at 1–2 ACH). Therefore, the 8-h experimental duration does not represent 8 h of real-world operation, but rather captures the full degradation process of the PCPs under continuous airflow. For dynamic response analysis (e.g., fan speed modulation or emergency scenarios), model results should be integrated with system-level simulations to account for temporal scaling effects.
(4) Limitations and Applicability: The scaled model focuses on the core heat and moisture exchange section and does not account for pressure losses or temperature gains along long ducts. When extrapolating to full-scale applications, additional safety factors should be applied to compensate for duct losses, and the total number of PCPs required should be recalculated based on the total airflow demand of the server room.

2.8. Evaluation index

The cooling capacity of the combined system is evaluated by the temperature difference between the inlet and outlet [42], that is ΔT_1

$$\Delta T_1 = T_{in} - T_{out} \tag{1}$$

The dehumidification performance of the combined system is evaluated by a change in humidity ratio (*d*) at the front and back of the PCP [43], that is Δd_1

$$\Delta d = d_{in} - d_{out} \tag{2}$$

Where d_{out} is the d of the outlet air, d_{in} is the d of the inlet air. When the tepperature and relative humidity are known, the *d* can be calculated by the following formula [44]:

$$d = [(622 \times p_v) / (p - p_v)] \tag{3}$$

Where p_v is the partial pressure of water vapor; *p* is the total pressure of the air.

The evaporation efficiency of the DEC equipment [45]:

$$\eta = \left[\left(T_{in} - T_{db,out}\right) / \left(T_{in} - T_{wb,in}\right)\right] \times 100\% \tag{4}$$

Where η is the direct water evaporative cooling efficiency (DEDEC); $T_{db,out}$ is the dry bulb temperature of the air after direct evaporation; $T_{wb,in}$ is the wet bulb temperature of the inlet air. Its value is calculated from the measured inlet air dry bulb temperature (T_{in}) and relative humidity (RH_{in}) based on the thermodynamic relations defined in the ASHRAE Fundamentals Handbook (2021).

The Cooling efficiency is evaluated by ΔT_1 and Tin.

$$\text{Cooling efficiency}(\beta) = \Delta T_1 / T_{in} \tag{5}$$

Where β is the Cooling efficiency.

The Dehumidification efficiency is evaluated by Δd_3 and d_p.

$$\text{Dehumidification efficiency} = \Delta d_3 / d_p \tag{6}$$

Where d_p is the dehumidification amount after evaporation.

2.9. Uncertainty analysis

Since the temperature and humidity of the natural environment simulated in the experiments have a slight fluctuation range, this will affect the reliability and accuracy of the experimental results. Using the method proposed by Moffat [46] to calculate the uncertainty of the experimental data, the relationship equation between the variable Y and the independent variables $x_1, x_2, \ldots\ldots x_n$ is expressed as follows:

$$Y = f(x_1, x_2 \ldots x_n) \tag{7}$$

The uncertainty of the parameter Y can be defined as follows [47]:

$$\sigma_Y = \sqrt{\left(\frac{\partial Y}{\partial x_1}\sigma_{x_1}\right)^2 + \left(\frac{\partial Y}{\partial x_2}\sigma_{x_2}\right)^2 + \cdots + \frac{\partial Y}{\partial n}\sigma_{x_n}\Big)^2} = \sqrt{\sum_1^n \left(\frac{\partial Y}{\partial x_i}\sigma_{x_i}\right)^2} \tag{8}$$

Where $\sigma_{x_1}, \sigma_{x_2}, \ldots\ldots\sigma_{x_n}$ are the uncertainties of $x_1, x_2, \ldots\ldots x_n$, respectively.

The relative uncertainty of parameter Y is expressed as [47]:

$$\sigma_r = (\sigma_Y / Y) \times 100\% \tag{9}$$

To quantify the influence of inlet temperature measurement error on the uncertainty of efficiency, the partial derivative of efficiency with respect to T_{in} is required. Differentiating Eq. (5) with respect to T_{in} and assuming that the outlet temperature T_{out} does not vary with inlet temperature (i.e., $\partial T_{out}/\partial T_{in} = 0$):

$$\frac{\partial \beta}{\partial x} = \frac{T_{in}\,\frac{\partial(\Delta T_1)}{\partial x} - \Delta T_{in}\,\frac{\partial T_{in}}{\partial x}}{T_{in}^2} \tag{10}$$

Since $\frac{\partial(T_{in}-T_{out})}{\partial T_{in}} = 1$ and $\frac{\partial T_{in}}{\partial T_{in}} = 1$, substituting these yields:

$$\frac{\partial \beta}{\partial T_{in}} = \frac{T_{in}\cdot 1 - (T_{in} - T_{out})\cdot 1}{T_{in}^2} = \frac{T_{out}}{T_{in}^2} \tag{11}$$

Equation (10) represents the partial derivative of cooling efficiency with respect to inlet temperature T_{in}. Where β is the Cooling efficiency, $\frac{\partial \beta}{\partial T_{in}}$ is Partial derivative of efficiency with respect to inlet temperature.

Table 4 shows the uncertainties of the measured and calculated parameters using the equipment and instrument specifications and the above formulas. To ensure data reliability over the 8-h experiments, all sensors were calibrated before and after each test, with mid-campaign spot checks (every 2 h) confirming no significant drift. Humidity sensors were protected from direct spray to prevent saturation, and energy balance consistency was verified for selected steady-state periods.

Table 4
The uncertainty of measured parameters and calculated parameters.

Parameters	Units	Uncertainty
Measured parameters		
T	°C	±0.1 °C
RH	%	±2.5%
v_a	m/s	0.02%
v_w	ml/min	±0.02%
Calculated parameters		
Cooling efficiency	%	±0.13%
η	%	±0.11%
Dehumidification efficiency	%	±0.2%

3. Result

3.1. Thermal performance of PCP

3.1.1. Energy storage capacity of the PCP

Fig.10 (a) plots the temperature curve of the PCM from the liquid state to the complete solidification. In the first 1.4 h, the PCM temperature decreases approximately linearly with time, which decreases by about 6 °C. The cold source at night is mainly stored by sensible heat through the PCM temperature drop. After 1.8 h, the PCM temperature first decreases and then tends to stabilize with the increase of time. This occurs when the PCM reaches its freezing point, undergoing a phase transition from liquid to a liquid-solid mixture, ultimately solidifying completely. The cold energy is mainly stored by the latent heat of phase change. Among them, the latent heat storage stage is maintained for about 5.2 h. During the period of 7 h~10 h, the temperature of PCM and T_{in} are the same, indicating that PCM has completely solidified. Therefore, when the temperature is 20 °C at night, the PCM needs to be completely solidified for about 7 h.

The total cold storage capacity of PCP is about 3431 kJ, of which the sensible heat stage is about 280.5 kJ, accounting for 8.2%. The latent heat stage was 3151 kJ, accounting for 91.8%. The total cold storage capacity of 3431 kJ, with a significant contribution from latent heat, indicates that the PCP can be highly effective in applications requiring energy storage and temperature control.

Fig.10 (b) plots the PCP temperature and liquid fraction during the melting process of the PCM. The PCP temperature increases approximately linearly during the first 1.5 h. Then, it slowly increases with the increase of experimental time. After 1 h, the liquid fraction nonlinear increases rapidly with time. From 5 h to 8 h, the temperature of the PCP tends to stabilize with a slow increase in time. The final liquid fraction reaches about 0.9, indicating that the mass of liquid from the PCM melting accounts for 90% of the total mass of PCM solids and liquid. Furthermore, the low thermal conductivity of paraffin wax (0.21 W/(m·K)) primarily accounts for the extended phase-change duration of 5–7 h (Fig. 10) and the gradual increase in liquid fraction. This material property restricts internal heat transfer within the PCM, leading to delayed thermal response under fluctuating loads, ineffective utilization of the full latent heat capacity, and consequently constrained transient cooling capability [48].

Energy Balance Validation: To verify the internal consistency between the cold energy stored in the PCP and the actual cooling effect delivered to the airflow, an energy balance check was performed for the effective cooling period identified in Section 3.1.2 (approximately 5.5 h, during which the inlet-outlet temperature difference $\Delta T_1 \geq 1.0$ °C).

Under the conditions of Case 1 (air supply velocity $v_a = 1.0$ m/s, DVC cross-section dimensions 0.65 m × 0.65 m, cross-sectional area $A = 0.4225$ m^2, air density $\rho_a = 1.2$ kg/m^3), the mass flow rate of air through the DVC is calculated as follows:

$$\dot{m}_a = \rho_a \cdot v_a \cdot A = 1.2 \times 1.0 \times 0.4225 = 0.507 \text{ kg/s}$$

Using the trapezoidal method to numerically integrate the $\Delta T_1(t)$ curve over the 5.5 h effective cooling period in Fig. 11, the average inlet-outlet temperature difference during this period is obtained as approximately 1.8 °C. Accordingly, the cooling energy delivered to the airflow can be calculated by the following equation:

$$Q_{air} = \dot{m}_a \cdot c_{p,a} \cdot \overline{\Delta T_1} \cdot t \tag{12}$$

where $c_{p,a} = 1.005$ kJ/(kg·K) is the specific heat of air, and $t = 5.5 \times 3600 = 19,800$ s is the effective cooling duration. Substituting the values yields: $Q_{air} = 0.507 \times 1.005 \times 1.8 \times 19,800 \approx 1820$ kJ.

This value represents the cold energy actually released by the PCP and transferred to the airflow during the effective cooling period, accounting for approximately 53% of the total cold storage capacity of the PCP (3431 kJ, see Section 3.1.1). The remaining cold energy (approximately 1611 kJ) is attributed to two main factors: firstly, the PCM was not completely melted by the end of the 8 h experiment (as shown in Fig. 10b, with a liquid fraction of 90%), meaning some cold energy remained stored in the PCM; secondly, a small amount of cold energy was lost to the environment due to imperfect insulation.

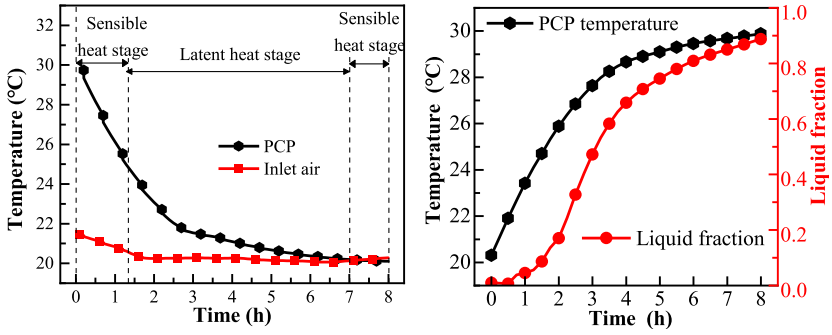

(a) Solidification process (b) Melting process

Fig. 10. Thermal performance curve of PCP.

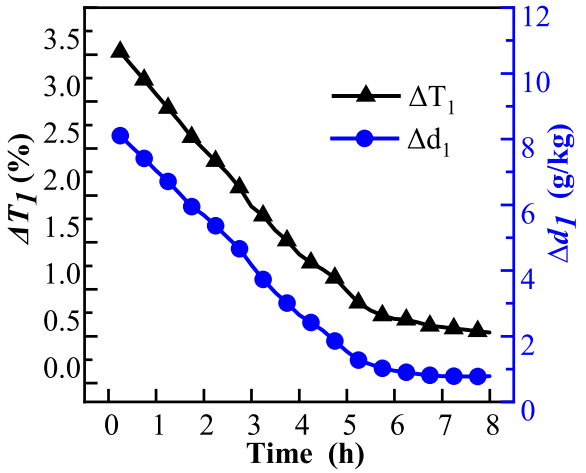

Fig. 11. Cooling and dehumidification performance curves of PCP.

The order-of-magnitude agreement between the delivered cooling energy (1820 kJ) and the total stored cold (3431 kJ), together with the 53% utilization rate being consistent with the PCM liquid fraction progression (Fig. 10b), confirms the internal consistency of the experimental measurements. This energy balance check demonstrates that the measured inlet-outlet temperature differences and airflow rates are physically consistent with the characterized cold storage capacity of the PCM.

3.1.2. Cooling and dehumidifying performance

The ΔT_1 is used to evaluate the cooling performance, and the Δd_1 is used to evaluate the dehumidification performance. The larger the values of these two indicators, the better the cooling and dehumidification performance of the PCP.

The cooling and dehumidification performance of the PCP system was evaluated under Case 1. As shown in Fig. 11, both performance indicators initially decline over time before stabilizing. The temperature difference ΔT_1 decreases rapidly from 3.2 °C to 0.7 °C during the first 5 h, then gradually levels off at approximately 0.5 °C. To define the effective operating period objectively, a threshold of $\Delta T_1 \geq 1.0$ °C was adopted, representing a practically meaningful cooling capability. Based on this criterion, the effective cooling duration of the PCP under these conditions is approximately 5.5 h, corresponding to the time interval in which ΔT_1 remains above the threshold in Fig. 11. Within the first hour, the outlet air temperature remains ≤27 °C, indicating that the PCP alone can temporarily satisfy the supply-air temperature requirements for data centers in this specific environment. This is because heat and moisture exchange between the PCP and the incoming hot air raises the PCM temperature, reducing the cooling effect (reflected in the decrease of ΔT_1). Once the PCP temperature exceeds the air dew point, it loses dehumidification ability. Before this point, dehumidification efficiency remained above 18.8% for over 5 h.

3.2. Performance comparison of two DEC systems

Fig. 12 plots the variation of T and RH of the air at the front and rear ends of the two DEC devices in T_{in} of 32 °C, RH_{in} of 50%, v_a of 3.0 m/s, and v_w of 80 ml/min operating conditions.

From Fig. 12 (a), it can be observed that after passing through the DEC device, the temperature of the inlet air decreases while the

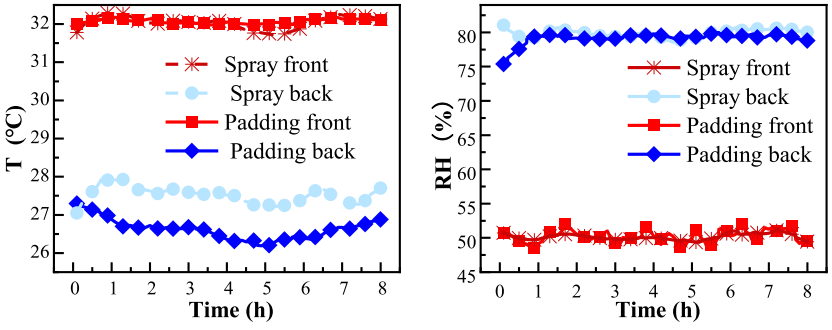

(a) The temperature after evaporative cooling **(b) The RH after evaporative cooling**

Fig. 12. Comparative performance curves of two DEC systems.

RH increases. Fig. 12 (b)shows that the RH both increased by about 30%. The average evaporative temperature drop of SDEC is 4.6 °C, and the η is 47.37%. While the average evaporative temperature drop of DPDEC is 5.5 °C, and the η is 57.90%. The evaporative temperature drop of DPDEC is about 0.9 °C more than that of SDEC.

Compared with the SDEC system, the DPDEC system enhances cooling performance by utilizing highly absorbent padding, primarily through increasing the water-air contact area and extending the contact time. However, as shown in Fig. 13, the padding requires a certain start-up period to become fully wetted and achieve optimal functionality. The wetting time—defined as the duration required to reach 95% of the steady-state relative humidity—was measured to be approximately 13 min. Consequently, under identical operating conditions, the cooling capacity of the DPDEC system is slightly lower than that of the SDEC system during the first 20 min. Achieving rapid wetting of the padding will contribute to improved cooling performance.

3.3. Performance comparison of two combined systems

Fig. 14 shows the temperature distribution at different positions within the DVC for separate experiments conducted using two combined systems: DPDEC-PCP and SDEC-PCP. As illustrated in the figure, under both operating conditions, a sharp temperature drop is observed at the 20 cm position. This occurs because the high-temperature air at this location passes through the DEC section, where sensible heat exchange with water takes place. During this heat and mass transfer process, the air temperature decreases while its humidity ratio increases. The DEC section exhibits greater cooling capacity under the DPDEC system across all tested conditions, further confirming its superior evaporative cooling performance. From the PCP section to the outlet, the DPDEC-PCP system maintains slightly lower temperatures than the SDEC-PCP system, with the former registering values approximately 0.5 °C lower than the latter.

Fig. 15 presents the effect of the DPDEC-PCP and SDEC-PCP systems on the cooling and dehumidification performance of the PCP under the same working conditions. As shown in Fig. 15a, ΔT_3 exhibits an approximately linear decreasing trend over time, gradually leveling off. In Fig. 15b, Δd_3 decreases sharply at first and then stabilizes, indicating that the performance of the PCP gradually weakens over time. Notably, both performance indicators follow the same trend under the two combined systems, with only marginal differences. This suggests that the configuration of the upstream system has a negligible impact on the PCP's performance.

In summary, although both system configurations have little effect on the PCP's performance, the DPDEC system achieves higher efficiency (η) for the same hydroelectric energy input, demonstrating superior cooling performance. Therefore, the DPDEC-PCP system represents a more effective configuration for cooling and dehumidification. Subsequent experiments on performance factor optimization were carried out using this combined system.

3.4. Sensitivity analysis

3.4.1. Effect of the t_{in}

Fig. 16 plots the effect of T_{in} variation on the performance of the system. From Fig. 16 (a) and (b) can be observed that both the T_{out}

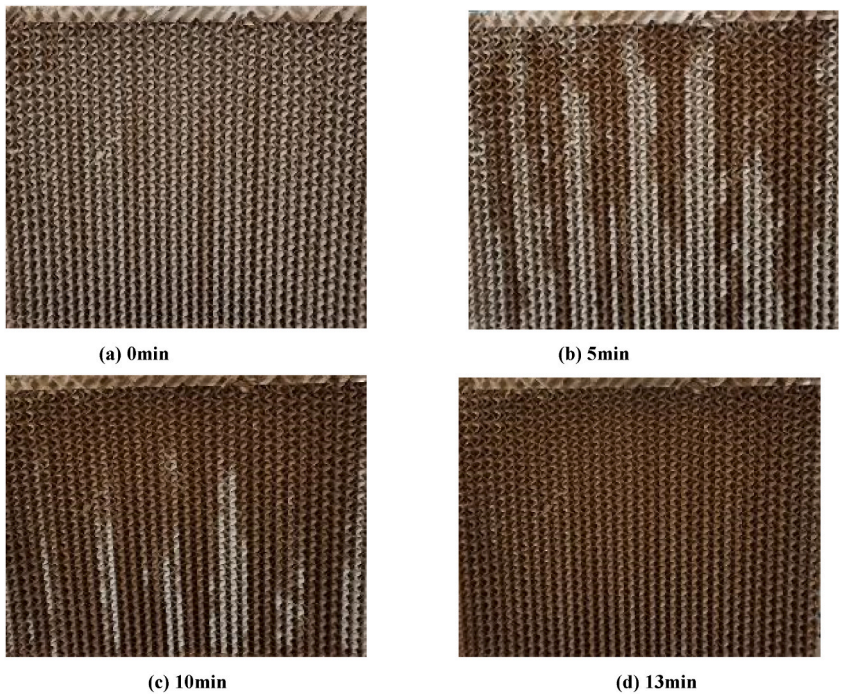

Fig. 13. The process of change of padding state with time.

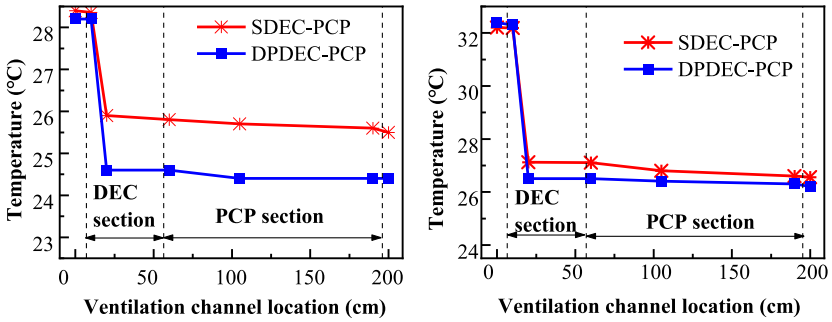

Fig. 14. Temperature distribution in DVC for DPDEC-PCP and SDEC-PCP systems.

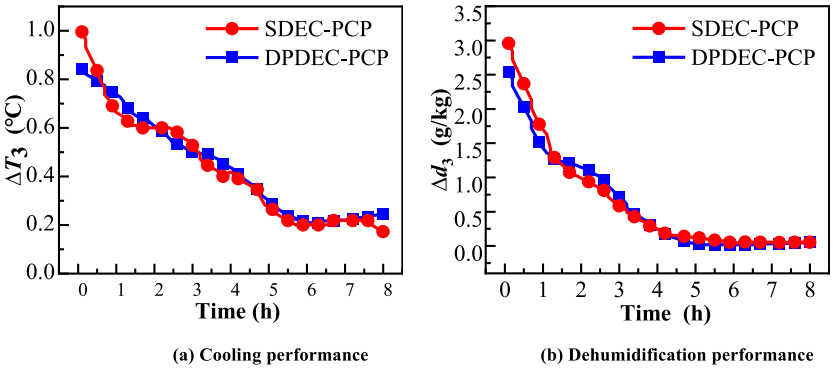

Fig. 15. Influence of two combined system types on PCP performance.

and RH_{out} gradually increase over time before eventually stabilizing when the T_{in} reaches or exceeds 36 °C. This is because the PCP plays the role of cooling and dehumidifying in the early stage, so the T_{out} and RH_{out} are low. When the RH_{in} is 50% and the T_{in} does not exceed 36 °C, this combined system is easy to meet the air supply temperature requirements of the machine room.

Among them, evaporative cooling increases with the increase of T_{in} as seen in Fig. 16 (c). T_{in} increases from 28 °C to 44 °C and the η changes from 58.12% to 90.45%, which indicates that the DEC is more effective in cooling in high temperatures. From Fig. 16 (d), it is found that with the increase of T_{in}, the RH after DPDEC is stabilized at about 80%. It indicates that the effect of T_{in} on evaporative humidification is not significant.

In addition, from Fig. 16 (e) and (f) can be seen that two performance indicators of the PCPs change over time. The change is not a simple linear trend, but a nonlinear pattern of accelerated reduction followed by gradual stabilization. T_{in} increases from 28 °C to 44 °C, and the cooling capacity of the PCP per meter improves from 0.5 °C to 3.5 °C in 1 h. With an RH_{in} of 50% and $T_{in} \geq 36$ °C, the PCP exhibits a significantly improved dehumidification effect. Where T_{in} increases from 36 °C to 44 °C, the dehumidification efficiency increases from 12.52% to 31.25%.

3.4.2. Effect of the RH_{in}

Fig. 17 plots the results of the influence of different RH_{in} on the system with the time. Fig. 17 (a) and (b) show that T_{out} and RH_{out} remain relatively stable when the RH_{in} is not exceed 30%. However, when RH_{in} exceeds 30%, both the T_{out} and RH_{out} exhibit a linear increase followed by stabilization over time. This indicates that higher levels of RH_{in} significantly influence the characteristics of the outlet air, resulting in noticeable changes in both temperature and humidity. Under the experimental condition, only the RH_{in} of 20% meets the data center air supply temperature requirement. However, the T_{out} is only about 1 °C higher than the standard requirement when the RH_{in} is not exceed 60%, which indicates that the system has good cooling performance.

From Fig. 17(c) and (d), we can see the law of the influence of the RH_{in} on the humidification and cooling performance of DPDEC. With the increase of the RH_{in}, the cooling performance of the system is weakened, and the Δd_2 is reduced. Fig.17 (e) plots the influence curves of RH_{in} on the cooling performance of PCP. The cooling performance index of the PCP undergoes an approximately linear process that first decreases and then tends to stabilize. In Fig. 17 (f), the RH_{in} is at 20% and 30%, the Δd_3 is close to 0. It indicates that the PCP has no dehumidifying effect under this condition. When the t RH_{in} exceeds 40%, the dew point temperature of the air at the front end of the PCP is much higher than the PCM temperature, resulting in a substantial increase in Δd_3. As RH_{in} increases, both the magnitude of Δd_3 and its duration also increase. This indicates that PCP has better dehumidification performance under high

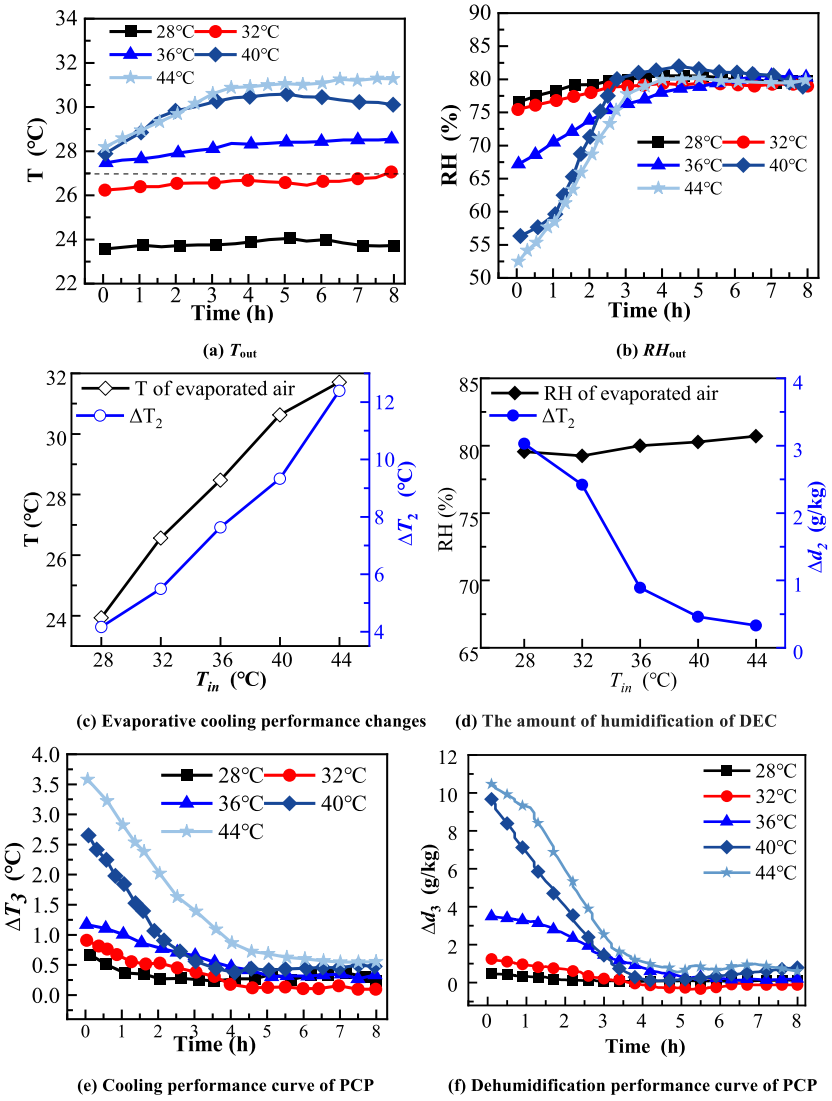

Fig. 16. Influence of different T_{in} on the performance of the combined system.

temperature and high humidity conditions.

3.4.3. *Effect of the air supply velocity*

The results of the effect of v_a on this combined system are shown in Fig. 18. Fig.18 (a) shows the pattern that the T_{out} increases in a linear relationship and the ΔT_1 decreases in a linear relationship as the v_a increases. This indicates that the v_a has a large influence on the cooling performance of the system. The cooling efficiency of the system is 29.84%, 27.78%, 25.83%, 24.44%, and 22.22% for five air speeds from small to large, respectively. Fig.18 (b) plots the variation curve of RH_{out} at different air supply velocities, from which it can be seen that the RH_{out} first increases and then tends to stabilize with time. Among them, the RH_{out} is almost below 80% when the air velocity exceeds 2.5 m/s. They meet the humidity requirement.

The pattern of v_a on DPDEC is seen in Fig. 18(c) and (d). From they can be observed that the ΔT_2 and the ΔRH_2 diminish rapidly as the v_a increases. The reason is that the increased v_a shortens the contact time between the air and the padding, and the air and water can not carry out sufficient heat and humidity exchange. However, When the v_a reaches 2.5 m/s and continues to increase, the influence on the humidification and cooling effect of DPDEC is not significant.

The effects of v_a on the cooling and dehumidifying performance of the PCP are plotted in Fig. 18(e) and (f). From them can be observed that the cooling and dehumidifying performance indexes of the PCP both show a nonlinear trend of first gradually decreasing and then stabilizing with time. The ΔT_3 and Δd_3 are comparable when the air velocity is set at 2.5 m/s and 3.0 m/s. The ΔT_3 at 2.5 m/s is higher by 0.5 °C, and the Δd_3 at this velocity is greater by 0.53 g/kg compared to the readings at 3.0 m/s. This suggests that the cooling and dehumidification performance of the PCP is more effective at lower air velocities.

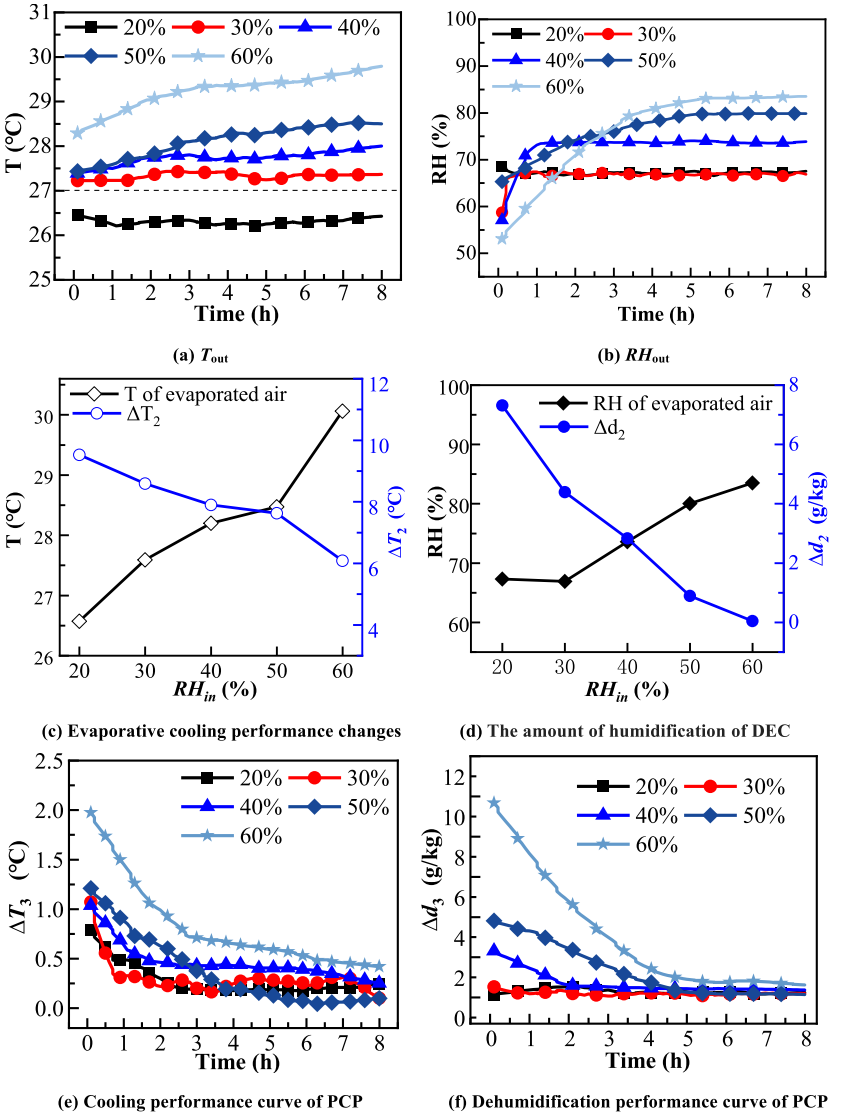

Fig. 17. Influence of different RH_{in} on device performance.

3.4.4. *Effect of the water flow*

Fig. 19 plots the change curves of T and RH after humidification and cooling by the padding at different v_w in the first 2 h. As shown in Fig. 19 (a), it can be seen that the RH of evaporated air rises rapidly with time and then closes to relative stability. According to the experimental observation, the padding has reached the wet state when the RH of air fluctuates within the range of 85% ± 2.5%. 40 ml/min, 60 ml/min, 80 ml/min, 100 ml/min and 120 ml/min to reach the wet state of the time of 28min, 22min, 16min, 13min and 7min. The v_w increases from 40 ml/min to 120 ml/min and the time to reach the wetted state is shortened by 21min.

Since the membrane becomes thoroughly wet, the effect of water flow rate on evaporation is minimal. Therefore, after the membrane is fully saturated at different flow rates, the flow rate can be uniformly adjusted to the minimum (40 ml/min) to calculate the total water consumption over an 8-h cycle. For example: 60 ml/min, Total water consumption = 60 × 22 + 40 × (480 − 22) = 19.6 L. Therefore, the water consumption corresponding to 40 ml/min, 80 ml/min, 100 ml/min, and 120 ml/min is 19.2 L, 19.84 L, 19.98 L, and 19.76 L.

As can be seen from Fig. 19 (b), the T of evaporated air decreases rapidly with time and then tends to stabilize. 10min ago, the temperature of the air after evaporation decreased slightly more with the increase in v_w. After 30 min, the evaporation temperature drop is almost the same for five different flow rates. It suggests that the flow rate of the padding after wetting has a small effect on the cooling and humidification of the DPDEC.

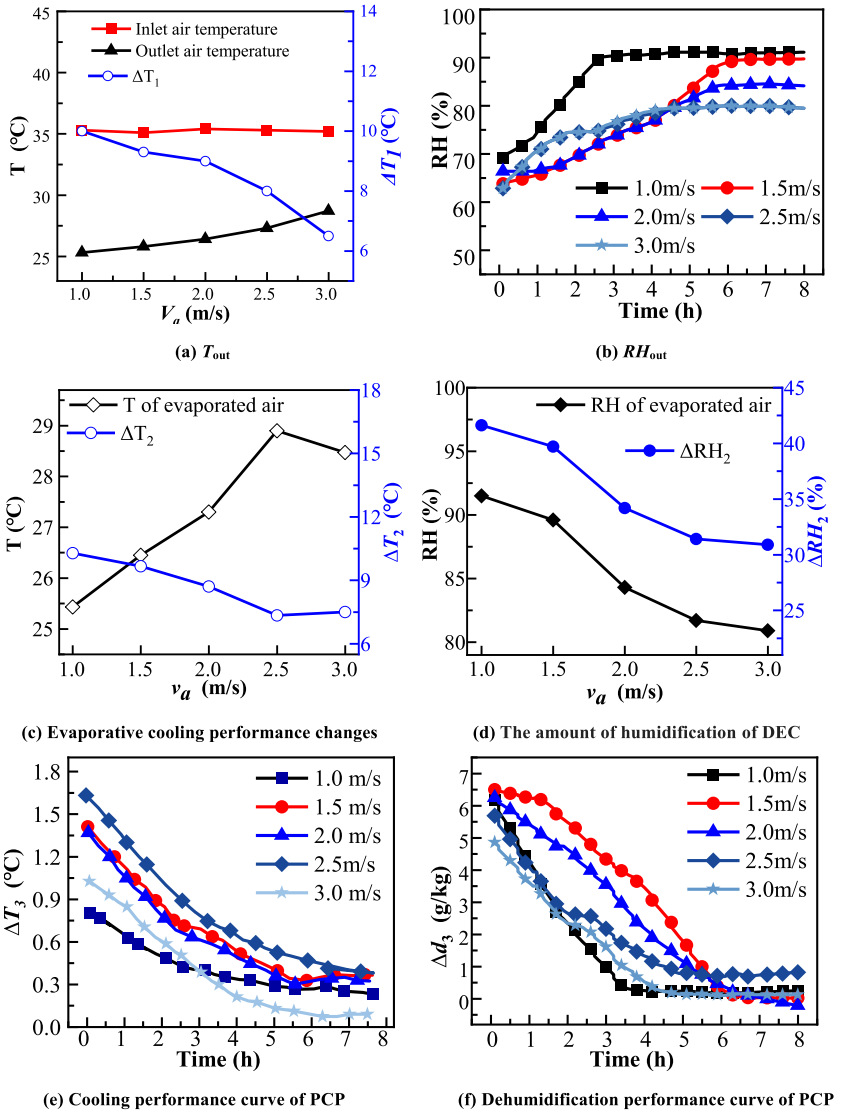

Fig. 18. Influence of different air supply velocities on device performance.

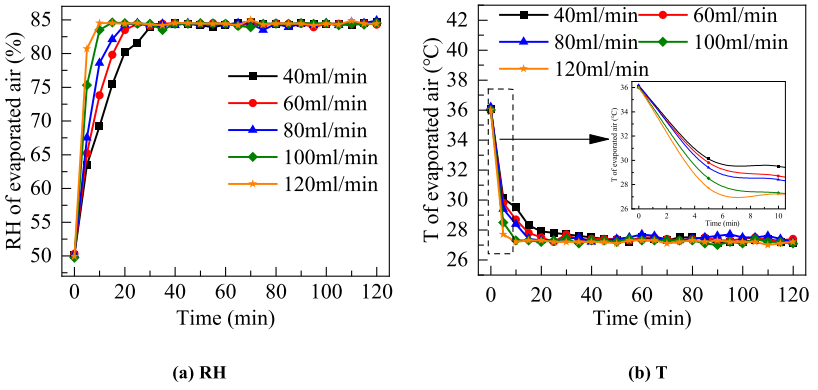

Fig. 19. Influence of different v_w on device performance.

4. Discussion

4.1. Analysis of optimization of system performance based on orthogonal experiment

4.1.1. Orthogonal experimental design

In the previous part, the influence of T_{in}, RH_{in}, $v_{a,}$ and v_w on the system was studied. To further optimize the cooling and dehumidification performance of the system, orthogonal experiments were carried out. Table 5 presents the orthogonal experimental design using an $L_{25}(5^5)$ orthogonal array with four factors and five levels to capture the nonlinear response characteristics observed in the single-factor experiments. The level values for each factor were determined based on actual operating conditions: inlet air temperature (IAT) ranges from 28 to 44 °C at 4 °C intervals, with the lower bound representing the threshold where free cooling becomes ineffective and the upper bound representing extreme high temperatures; inlet relative humidity (IRH) ranges from 20% to 60% at 10% intervals, covering the typical summer humidity range in Guiyang; air supply velocity (ASV) ranges from 1.0 to 3.0 m/s at 0.5 m/s intervals, corresponding to the full-scale design airflow velocity range; water flow rate (WF) ranges from 40 to 120 mL/min at 20 mL/min intervals, based on rotameter limits and padding wetting characteristics—below 40 mL/min results in insufficient wetting, while above 120 mL/min yields diminishing returns. The experiments use ΔT_1 and Δd_1 as the evaluation indexes, see Table 5.

4.1.2. Comprehensive results of range analysis and ANOVA

Based on the experimental data, the mean values of performance indicators at different factor levels, along with the range and ANOVA results, are presented in Tables 6 and 7.

From the combined results of Tables 6 and 7, the following conclusions can be drawn:

Regarding the influence on cooling effect (ΔT_1): Inlet Air Temperature (IAT) is the overwhelmingly dominant factor. Its range (9.72) is substantially higher than those of the other factors, and its ANOVA contribution rate reaches 94.6%, with high statistical significance ($F = 72.5$, $p < 0.01$). In contrast, the influence of Air Supply Velocity (ASV), Inlet Relative Humidity (IRH), and Wind Flow (WF) is relatively minor, and none reached statistical significance.

Regarding the influence on dehumidification effect (Δd_1): Inlet Relative Humidity (IRH) is the most critical factor, exhibiting the highest range (6.30) and contribution rate (62.8%), and is highly statistically significant ($F = 21.2$, $p < 0.01$). Inlet Air Temperature (IAT) also has a significant influence (contribution rate 29.3%, $F = 9.9$, $p < 0.05$), making it a secondary key factor. The influences of Air Supply Velocity (ASV) and Wind Flow (WF) are relatively small and not significant.

From Fig. 20, it is seen that ΔT_1 increases approximately linearly as the T_{in} increases. This shows that the more the system is used in high-temperature areas, the better the performance and the more cost-effective it will be. Whereas, ΔT_1 slowly and gradually decreases with the increase of RH_{in} and v_a. V_w has almost no effect on ΔT_1. The optimum solution to achieve temperature reduction is $T_{in} = 44$ °C, $RH_{in} = 20\%$, $v_a = 1.0$ m/s, and $v_w = 40$ ml/min. However, dehumidification did not reach the best solution when the optimum cooling effect was achieved. Taking into account the dehumidification, the system is recommended to be applied with a low air velocity and a smaller v_w in a natural environment with high temperature and high humidity. We can see that the order of influence on the ΔT_1 is $T_{\text{in}} > v_a > RH_{\text{in}} > v_w$. The Δd_1 is in the following order: $RH_{\text{in}} > T_{\text{in}} > v_a > v_w$.

Table 5

Case	T_{in} (°C)	RH_{in} (%)	v_a (m/s)	v_w (ml/min)	ΔT_1 (°C)	Δd_1 (g/kg)
1	28	20	1	40	6.9	0.2
2	28	30	2	100	5.5	0.1
3	28	40	3	60	3.8	0.4
4	28	50	1.5	120	3.7	0.5
5	28	60	2.5	80	3.4	2.2
6	32	20	3	100	6.7	0.2
7	32	30	1.5	60	7.1	0.9
8	32	40	2.5	120	6.8	0.2
9	32	50	1	80	7.5	3.8
10	32	60	2	40	6.8	4.5
11	36	20	2.5	60	9.3	0.2
12	36	30	1	120	10.9	0.6
13	36	40	2	80	9.1	5.1
14	36	50	3	40	9	4.0
15	36	60	1.5	100	9.5	9.1
16	40	20	2	120	13.1	0.3
17	40	30	3	80	12.2	0.7
18	40	40	1.5	40	12.9	1.1
19	40	50	2.5	100	11.1	1.7
20	40	60	1	60	13.2	7.8
21	44	20	1.5	80	14.8	0.1
22	44	30	2.5	40	14.1	1.6
23	44	40	1	100	15.1	6.8
24	44	50	2	60	14.4	8.1
25	44	60	3	120	13.5	8.9

Table 6
Factor analysis results for ΔT_1 (cooling effect).

Factor	Mean Values (Levels 1–5)	Range (R)	ANOVA F-value	Contribution Rate(%)	Significance ($\alpha = 0.05$)
IAT	4.66, 6.98, 9.38, 12.5, 14.38	9.72	72.5	94.6	Highly Significant ($p < 0.01$)
ASV	10.88, 9.7, 9.84, 9.14, 9.06	1.82	2.43	3.2	Not Significant
IRH	10.16, 9.94, 9.16, 9.16, 8.88	1.28	1.25	1.6	Not Significant
WF	9.54, 9.84, 9.88, 10.04, 9.36	0.68	0.36	0.5	Not Significant

Table 7
Factor analysis results for Δd_1 (dehumidification effect).

Factor	Mean Values (Levels 1–5)	Range (R)	ANOVA F-value	Contribution Rate(%)	Significance ($\alpha = 0.05$)
IRH	0.2, 0.82, 1.72, 3.74, 6.5	6.3	21.2	62.8	Highly Significant ($p < 0.01$)
ITA	0.68, 1.92, 3.9, 2.32, 5.1	4.42	9.9	23.9	Significant ($p < 0.05$)
ASV	3.78, 2.18, 2.6, 1.06, 2.52	2.72	2.0	5.9	Not Significant
WF	2.04, 2.7, 3.24, 3.08, 3.04	1.2	0.6	1.8	Not Significant

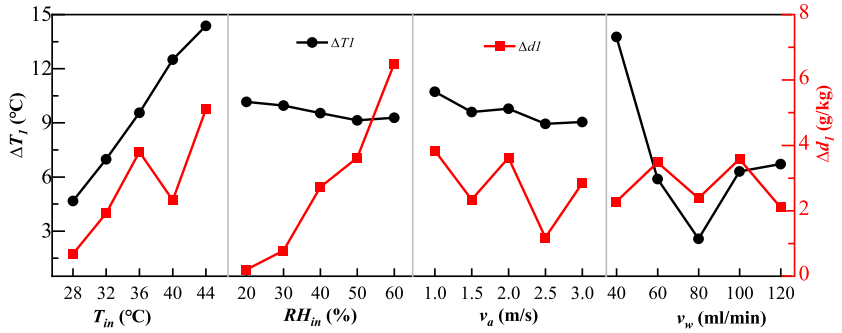

Fig. 20. The trend of different factors on indicators.

4.2. Analysis of matching system cooling capacity with data center demand

4.2.1. System cooling capacity with data center demand

Compared with a data center in Guiyang that also uses a direct ventilated air conditioning cooling system to evaluate the cooling capacity of the system. The data center needs 3456 m^3/h of outdoor fresh air, the fresh air temperature range is 28 °C~34 °C.

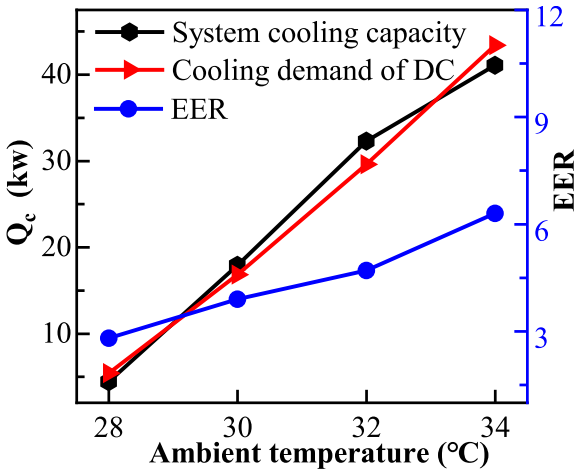

Fig. 21. Matching comparison between system cooling capacity and DATA CENTER demand at different temperatures.

Therefore, it required cooling capacity is 5.4 KW∼43.4 KW.

The overall system Energy Efficiency Ratio in this study is calculated based on the following formula:

$$EER = \frac{Q_c}{P_{total}} \tag{13}$$

Where Q_c is the measured total cooling capacity (kW) of the system; P_{total} is the total electrical power input (kW) to the cooling system required to deliver the aforementioned cooling, the electricity input includes the pump and the fan, calculated as 8-h average values.

From Fig. 21, it can be observed that at the outside temperature of 28 °C, the cooling capacity of the combined system is slightly below the cooling demand of the data center. However, the combined system's cooling capacity aligns with the data center's requirements as the temperature increases from 30 °C to 32 °C. Moreover, the energy efficiency ratio (EER) of the combined system improves as the outside temperature rises. In typical air conditioning and refrigeration systems, the EER generally ranges from 2.5 to 5.0. In contrast, this combined system can achieve a EER as high as 6.3. This elevated EER indicates that the system can significantly reduce the energy consumption of data centers during periods of high temperatures [49].

Overall, the ability of the combined system to meet the cooling needs of data centers, particularly as temperatures rise. Along with its high EER, highlights its potential for energy savings and improved performance in demanding environments.

4.2.2. Integration of the DPDEC-PCP system into actual data center layouts

This study presents lab-scale validation, but practical deployment requires consideration of system integration, airflow management, and redundancy design. In practical applications, the system would function as a dedicated air handling unit: outdoor air is pre-cooled by the DEC section, then further cooled and dehumidified by parallel PCP arrays. The conditioned air collects in a plenum and is delivered to server racks via perforated floor tiles (underfloor supply) or overhead ducts (overhead supply). A 45 cm spacing between the DEC and PCP sections is maintained to ensure uniform airflow distribution.

To optimize airflow organization, cold/hot aisle containment should be implemented to prevent mixing of cold and hot air. Server fans should coordinate with central DVC fans, with the thermal mass of PCPs buffering load fluctuations. The number and open area of perforated tiles should be calculated based on total airflow demand (1728–3456 m^3/h). For reliability, multiple PCP banks should be arranged in parallel to meet the target airflow, with N+1 redundancy: backup pumps and padding for the DEC section, parallel PCP banks ensuring that failure of one bank reduces cooling capacity by no more than 25%, and multiple parallel fans guaranteeing that failure of any single fan maintains airflow at ≥80% of design capacity. PCPs should be rail-mounted to support hot-swap replacement. The control system must monitor outdoor conditions, PCP state of charge, cold/hot aisle temperature and humidity, and IT load to enable intelligent switching between free cooling, hybrid, and mechanical cooling modes. Future work should include material durability testing, full-scale demonstration, and cost-benefit analysis.

In practice, the system would integrate with existing CRAH/CRAC units through a staged control strategy: Mode 1 (Free cooling): When ambient conditions are favorable ($T_{amb} \leq 32$°C, $RH_{amb} \leq 60\%$), the DPDEC-PCP system handles the full load; CRAH/CRAC units remain standby. Mode 2 (Hybrid): As conditions exceed the system's effective range, mechanical cooling provides supplemental cooling, with PCPs still contributing to pre-cooling. Mode 3 (Mechanical only): Under extreme conditions or during PCP nighttime regeneration, conventional cooling takes over [50].

The thermal mass of PCPs provides inherent buffering against IT load fluctuations, smoothing supply temperature variations during transient spikes. This passive inertia reduces mechanical cooling activation frequency. Regarding PUE impact: when operating in Mode 1, the system's high EER (up to 6.3) versus conventional cooling (EER 2.5–5.0) translates to significant energy savings. Assuming 6–8 h of daily Mode 1 operation during summer, annualized cooling energy reduction could lower overall data center PUE by an estimated 0.1–0.15, depending on climate and load profiles. Practical implementation requires a control system monitoring ambient conditions, PCP state of charge, server inlet temperatures, and IT load to optimize mode transitions.

Table 8
Compared with other cooling and dehumidification methods studied in data center.

Methods	Cooling efficiency	Dehumidification efficiency	Advantage	Disadvantage
Water-cooled air conditioner [51]	High	None	Consumes less power	High water consumption
Cold mist DEC [25]	Very high	None	The η is improved	The humidity exceeds the standard
Nature air cooling [15]	High	None	Very efficient and environmentally friendly	Susceptible to the external environment
PCES [39]	Middle	None	Sometimes, the refrigeration is zero energy consumption	At high temperatures does not meet DATA CENTER requirements
Thermosiphon loop - PCES [35]	Middle	Lower	Can be used for emergency cooling for a short time	High maintenance costs
PCES - DPDEC	Very high	Middle	Not only cooling but also dehumidifying	The initial investment is large

4.3. Analysis of the innovation of this combined system

Compared with similar studies on data center cooling technology and solutions, the innovations of this study are analyzed as follows. Compared the system with predecessors, see Table 8. The innovation of the research system was analyzed through four aspects: cooling efficiency, dehumidification efficiency, advantages, and disadvantages.

First, perform an overall system performance analysis. The cooling efficiency of the combined system was rated as 'very high', which significantly exceeded that of the other systems. The dehumidification efficiency of the system was evaluated as 'medium' which, although not significant, indicated an improvement in its dehumidification capability. In practical operation, the performance of the phase change panel dehumidification system is constrained by three dynamic factors: the nighttime regeneration of paraffin is dependent on weather conditions, where humid environments can lead to performance degradation; fluctuations in external temperature and humidity may induce partial phase changes, reducing moisture absorption efficiency; and material thermal inertia can cause misalignment in dehumidification/regeneration timing. The practical application of this technology requires consideration of its cyclic stability under long-term climatic fluctuations.

Second, the advantages and disadvantages of the system are analyzed. The system not only provides cooling but also dehumidification, thereby enhancing its versatility and practicality. Regarding low power consumption, this indicates the potential for significant savings on electricity bills over time. However, the substantial initial investment may pose a barrier to adoption by potential users.

Overall, the innovation of the system is primarily reflected in two key aspects. On one hand, the system can simultaneously cool and dehumidify, a capability that is relatively rare among mainstream systems available today. Conversely, the system offers significant advantages over other systems concerning cooling and energy efficiency.

4.4. Limitations and Future Research Directions

This study has validated the performance advantages of the DPDEC-PCP integrated cooling system in terms of thermodynamic principles and under ideal conditions. However, several key challenges must be addressed for practical engineering applications:

(1) Limitations in Long-term Reliability of Materials and System: Phase Change Materials (PCM) are subject to performance degradation risks during long-term phase change cycles, primarily including material phase separation, reduction in latent heat capacity, and changes in thermal conductivity [52]. Additionally, encapsulation structures may experience fatigue or sealing failure under thermal stress cycling, posing potential leakage risks [53]. The Indirect Evaporative Cooling (DEC) component is significantly affected by water quality. Under hard water conditions, scaling can easily occur, leading to reduced heat exchange efficiency. Moist surfaces may also foster microbial contamination, increasing system maintenance costs and health risks [54].
(2) System Dependence on Climatic Conditions: The energy-saving effectiveness of the system is highly dependent on the availability of "night cooling" or low-temperature periods. It performs excellently in dry or temperate climate zones with large diurnal temperature variations and prolonged low-temperature periods. However, in hot and humid climates with small diurnal temperature fluctuations, the window for natural cooling is limited, necessitating reliance on backup refrigeration systems. This impacts overall energy-saving benefits and the system's applicability range [55].
(3) Future Research Directions: Reliability Enhancement Studies: Conduct accelerated aging tests for PCM and encapsulation durability experiments to establish predictive models for performance degradation. Investigate anti-scaling treatment technologies and microbial control strategies for the DEC component. Climate Adaptability Optimization: Develop a system applicability evaluation model based on meteorological data from different regions to define geographical applicability boundaries. Create hybrid control strategies that complement mechanical refrigeration to expand the system's applicability range. Engineering Empirical Research: Implement medium-to long-term pilot operations in actual data centers to monitor the system's energy efficiency performance, maintenance requirements, and operational costs under dynamic loads and real climatic conditions.

These research directions will advance the technology from laboratory validation to engineering application, providing a practical and feasible solution for green cooling in data centers.

5. Conclusion

Data center consumes very high energy, especially in summer. This study demonstrated the DPDEC-PCP system to further optimize the efficiency of handling hot outdoor air. Firstly, the ability of PCM to store cold was experimentally investigated. Secondly, two kinds of combined systems were experimentally investigated to optimize the cooling and dehumidification performance. Finally, based on the conclusions of the previous step, the effects of IAT, IRH, ASV, and WF on the performance of the system were investigated. At the same time, orthogonal experiments were used to analyze the primary and secondary influences on the cooling and dehumidifying performance of the combined system. The main conclusions of this work are as follows:

(1) When the ASV is 3 m/s, the WF is 80 ml/min, the IRH is 60%, and IAT increases from 28 °C to 44 °C, the cooling efficiency of the system increases by 31.43%.

(2) When the ASV is 3 m/s, the IAT is 36 °C and the IRH is 60%, the system makes the outlet air temperature at a temperature of 27 °C and a outlet relative humidity of 62.3%. Separately, the air is lower by 6.6 °C by the DPDEC and 2.4 °C by the PCPs, and the d increases by 24.3% through evaporation but decreases by 22% through the PCPs.
(3) The system has a good dehumidification capability in 1～3 h under experimental conditions when the IRH ≥40%. Subsequently, the system will lose its dehumidifying ability when the PCM temperature is higher than the dew point temperature of the air at the front of the PCP.
(4) When the ASV is increased from 2.5 m/s to 3.0 m/s, the cooling efficiency of the system decreases by 7.62%, and the dehumidification effect is weakened to some extent. After the filler is wetted, the WF has a weak effect on the system performance.
(5) The main factors affecting the cooling performance of the system are IAT > ASV > IRH > WF in order, and for the dehumidification performance are IRH > IAT > ASV > WF.

CRediT authorship contribution statement

Yangyang Zhang: Writing – review & editing, Writing – original draft, Formal analysis, Data curation, Conceptualization. **Hongli Xu:** Writing – review & editing, Data curation, Conceptualization. **Jiri Zhou:** Writing – review & editing. **Xing Liang:** Writing – review & editing. **Hongwei Wu:** Writing – review & editing. **Ruiyong Mao:** Writing – review & editing, Methodology. **Zujing Zhang:** Writing – review & editing, Resources, Investigation, Funding acquisition.

Declaration of competing interest

We declare that we have no financial and personal relationships with other people or organizations that can inappropriately influence our work, there is no professional or other personal interest of any nature or kind in any product, service and/or company that could be construed as influencing the position presented in, or the review of, the manuscript entitled '***Experimental investigation on thermal and moisture performance of direct evaporative cooling coupled with phase change plates for data centers***'.

Acknowledgments

The author would like to thank the financial support of the National Natural Science Foundation of China (NO.52168013), Guizhou Provincial Basic Research Program Project (NO. ZD [2026] 040) and the Guizhou Province Postgraduate Research Fund Project (NO. 2024YJSKYJJ114).

Data availability

Data will be made available on request.

References

[1] K. Brzozowska-Rup, M. Nowakowska, M. Zdradzisz, Cloud computing in the Polish public administration: current state and development prospects, Technol. Forecast. Soc. Change 205 (2024) 123500, https://doi.org/10.1016/j.techfore.2024.123500.
[2] J. Cho, J.H. Moon, Numerical coupling of energy efficiency and thermal performance for cold plate cooling optimization in high-density compute AI data centers, Energy Build. (2025) 116441, https://doi.org/10.1016/j.enbuild.2025.116441.
[3] J. Wen, H.-T. Yin, C.-P. Chang, K. Tang, How AI shapes greener futures: comparative insights from equity vs debt investment responses in renewable energy, Energy Econ. 136 (2024) 107700, https://doi.org/10.1016/j.eneco.2024.107700.
[4] W. Yan, H. Kao, U. Sajjad, C. Li, S. Rashidi, Experimental study on thermal management of data center with non-uniform heat load, Case Stud. Therm. Eng. 73 (2025) 106578, https://doi.org/10.1016/j.csite.2025.106578.
[5] Y. Zhang, H. Li, S. Wang, Life-cycle optimal design and energy benefits of centralized cooling systems for data centers concerning progressive loading, Renew. Energy 230 (2024) 120847, https://doi.org/10.1016/j.renene.2024.120847.
[6] D. Mytton, M. Ashtine, Sources of data center energy estimates: a comprehensive review, Joule 6 (2022) 2032–2056, https://doi.org/10.1016/j.joule.2022.07.011.
[7] E. Masanet, A. Shehabi, N. Lei, S. Smith, J. Koomey, Recalibrating global data center energy-use estimates, Science 367 (2020) 984–986, https://doi.org/10.1126/science.aba3758.
[8] J. Zhang, R. Mao, C. Li, J. Lan, X. Yi, Z. Zhang, Optimization air-conditioning system and thermal management of data center via fan-wall free cooling technology, Appl. Therm. Eng. 234 (2023) 121245, https://doi.org/10.1016/j.applthermaleng.2023.121245.
[9] V. Depoorter, E. Oró, J. Salom, The location as an energy efficiency and renewable energy supply measure for data centres in Europe, Appl. Energy 140 (2015) 338–349, https://doi.org/10.1016/j.apenergy.2014.11.067.
[10] Y. Zhang, K. Shan, X. Li, H. Li, S. Wang, Research and Technologies for next-generation high-temperature data centers – State-of-the-arts and future perspectives, Renew. Sustain. Energy Rev. 171 (2023) 112991, https://doi.org/10.1016/j.rser.2022.112991.
[11] M. Kuzay, A. Dogan, S. Yilmaz, O. Herkiloglu, A.S. Atalay, A. Cemberci, C. Yilmaz, E. Demirel, Retrofitting of an air-cooled data center for energy efficiency, Case Stud. Therm. Eng. 36 (2022) 102228, https://doi.org/10.1016/j.csite.2022.102228.
[12] N.L. Boafo, S. Boahen, J.M. Choi, Performance optimization and energy analysis of a proposed data center dual-mode air source cooling system on the mode change temperature, Case Stud. Therm. Eng. 74 (2025) 106957, https://doi.org/10.1016/j.csite.2025.106957.
[13] L. Silva-Llanca, C. Ponce, E. Bermúdez, D. Martínez, A.J. Díaz, F. Aguirre, Improving energy and water consumption of a data center via air free-cooling economization: the effect weather on its performance, Energy Convers. Manag. 292 (2023) 117344, https://doi.org/10.1016/j.enconman.2023.117344.
[14] R. Madurai Elavarasan, M. Nadarajah, R. Pugazhendhi, S. Gangatharan, An experimental investigation on coalescing the potentiality of PCM, fins and water to achieve sturdy cooling effect on PV panels, Appl. Energy 356 (2024) 122371, https://doi.org/10.1016/j.apenergy.2023.122371.
[15] Y. Zhou, Z. Wang, F. Wei, S. Li, J. Liu, D. Yu, Sustainability of direct air-side free cooling data centers in China: an assessment based on operational optimization, Appl. Therm. Eng. 273 (2025) 126462, https://doi.org/10.1016/j.applthermaleng.2025.126462.

[16] A. Aili, W. Long, Z. Cao, Y. Wen, Radiative free cooling for energy and water saving in data centers, Appl. Energy 359 (2024) 122672, https://doi.org/10.1016/j.apenergy.2024.122672.
[17] Y. Zhang, Z. Wei, M. Zhang, Free cooling technologies for data centers: energy saving mechanism and applications, Energy Proc. 143 (2017) 410–415, https://doi.org/10.1016/j.egypro.2017.12.703.
[18] Yongcheng Zhou, Shuangxiu Li, Qiang Li, Fanchao Wei, Dazhi Yang, Jinfu Liu, Daren Yu, Energy savings in direct air-side free cooling data centers: a cross-system modeling and optimization framework, Energy Build. 308 (2024).
[19] Y. Yu, L. Wang, Solid sorption heat pipe coupled with direct air cooling technology for thermal control of rack level in internet data centers: design and numerical simulation, Int. J. Heat Mass Tran. 145 (2019) 118714, https://doi.org/10.1016/j.ijheatmasstransfer.2019.118714.
[20] W.L. Wang, Y. Li, K. Lee, Effects of airflow distribution changes on the thermal environment of IT equipment in data centers, Case Stud. Therm. Eng. 73 (2025) 106604, https://doi.org/10.1016/j.csite.2025.106604.
[21] A. Keçebas, M. Ertürk, Advancing cooling load assessment in solar-intensive climates: a ΔT-based solar-air temperature approach for enhanced free cooling modeling, Energy Build. 345 (2025) 116095, https://doi.org/10.1016/j.apenergy.2025.116095.
[22] J. Xu, Y. Li, R.Z. Wang, W. Liu, P. Zhou, Experimental performance of evaporative cooling pad systems in greenhouses in humid subtropical climates, Appl. Energy 138 (2015) 291–301, https://doi.org/10.1016/j.apenergy.2014.10.061.
[23] Y. Lee, K. Chen, W. Yan, Y. Shih, C. Chao, Evaporative cooling method to improve energy management of overhead downward flow-type data center, Case Stud. Therm. Eng. 45 (2023) 102998, https://doi.org/10.1016/j.csite.2023.102998.
[24] A.R. Al-Badri, A.A.Y. Al-Waaly, The influence of chilled water on the performance of direct evaporative cooling, Energy Build. 155 (2017) 143–150, https://doi.org/10.1016/j.enbuild.2017.09.021.
[25] C. Li, R. Mao, Y. Wang, J. Zhang, J. Lan, Z. Zhang, Experimental study on direct evaporative cooling for free cooling of data centers, Energy 288 (2024) 129889, https://doi.org/10.1016/j.energy.2023.129889.
[26] J. Chu, X. Huang, Research status and development trends of evaporative cooling air-conditioning technology in data centers, Energy and Built Environment 4 (2023) 86–110, https://doi.org/10.1016/j.enbenv.2021.08.004.
[27] A. Alrashidi, S. Abdo, M.A. Abdelrahman, A.A. Altohamy, I.M.M. Elsemary, Thermal regulation for buildings using evaporative cooling technique: experimental study, Case Stud. Therm. Eng. 61 (2024) 104891, https://doi.org/10.1016/j.csite.2024.104891.
[28] Y. Jing, X. Xie, Y. Jiang, Performance comparison and suitable climatic zones of three water-mediated evaporative cooling technologies, Energy Convers. Manag. 277 (2023), https://doi.org/10.1016/j.enconman.2022.116637.
[29] P. Zhang, K. Li, Q. Liu, Q. Zou, R. Liang, L. Qin, Y. Wang, Thermal stratification characteristics and cooling water shortage risks for pumped storage reservoir–green data centers under extreme climates, Renew. Energy 229 (2024) 120697, https://doi.org/10.1016/j.renene.2024.120697.
[30] A. Waqas, Z. Ud Din, Phase change material (PCM) storage for free cooling of buildings—A review, Renew. Sustain. Energy Rev. 18 (2013) 607–625, https://doi.org/10.1016/j.rser.2012.10.034.
[31] S. Rostami, M. Afrand, A. Shahsavar, M. Sheikholeslami, R. Kalbasi, S. Aghakhani, M.S. Shadloo, H.F. Oztop, A review of melting and freezing processes of PCM/nano-PCM and their application in energy storage, Energy 211 (2020) 118698, https://doi.org/10.1016/j.energy.2020.118698.
[32] K. Nithyanandam, R. Pitchumani, Optimization of an encapsulated phase change material thermal energy storage system, Sol. Energy 107 (2014) 770–788, https://doi.org/10.1016/j.solener.2014.06.011.
[33] M.A. Said, H. Hassan, Parametric study on the effect of using cold thermal storage energy of phase change material on the performance of air-conditioning unit, Appl. Energy 230 (2018) 1380–1402, https://doi.org/10.1016/j.apenergy.2018.09.048.
[34] Y. Zhu, G. Englmair, H. Huang, J. Dragsted, Y. Yuan, J. Fan, S. Furbo, Numerical investigations of a latent thermal energy storage for data center cooling, Appl. Therm. Eng. 236 (2024) 121598, https://doi.org/10.1016/j.applthermaleng.2023.121598.
[35] X. Ma, Q. Zhang, S. Zou, An experimental and numerical study on the thermal performance of a loop thermosyphon integrated with latent thermal energy storage for emergency cooling in a data center, Energy 253 (2022) 123946, https://doi.org/10.1016/j.energy.2022.123946.
[36] B. Huang, Z. Zheng, G. Lu, X. Zhai, Design and experimental investigation of a PCM based cooling storage unit for emergency cooling in data center, Energy Build. 259 (2022) 111871, https://doi.org/10.1016/j.enbuild.2022.111871.
[37] J.-X. Wang, J. Qian, N. Wang, H. Zhang, X. Cao, F. Liu, G. Hao, A scalable micro-encapsulated phase change material and liquid metal integrated composite for sustainable data center cooling, Renew. Energy 213 (2023) 75–85, https://doi.org/10.1016/j.renene.2023.05.106.
[38] X. Gao, Y. Xiao, P. Gao, Z. Zhang, M. Sun, Experimental study of the effect of high humidity on the phase change plate thermal storage under natural convection, Energy 256 (2022) 124645, https://doi.org/10.1016/j.energy.2022.124645.
[39] L. Yang, H. Wu, Z. Zhang, R. Mao, J. Zhou, X. Liang, Experimental investigation on application potential of phase change assisted direct ventilation cooling system for Gui'an data center, Appl. Therm. Eng. 254 (2024) 123932, https://doi.org/10.1016/j.applthermaleng.2024.123932.
[40] A. Sathishkumar, P. Sundaram, R. Prabakaran, M. Cheralathan, J.H. Kim, S.C. Kim, Thermal performance evaluation of encapsulation materials for organic PCM-based cool thermal energy storage systems, Case Stud. Therm. Eng. 74 (2025) 106945, https://doi.org/10.1016/j.csite.2025.106945.
[41] W. He, Q. Xu, S. Liu, T. Wang, F. Wang, X. Wu, Y. Wang, H. Li, Analysis on data center power supply system based on multiple renewable power configurations and multi-objective optimization, Renew. Energy 222 (2024) 119865, https://doi.org/10.1016/j.renene.2023.119865.
[42] Y. Xu, M. Tian, C. Yan, D. Li, T. Deng, P. Guo, K. Hu, A data center energy efficiency optimization method based on optimal temperature control of designated active servers, Energy Build. 345 (2025) 116126, https://doi.org/10.1016/j.enbuild.2025.116126.
[43] G. Huang, M. Xie, Y. Zhao, T. Jia, Y. Dai, Experimental study on waste heat recovery process in a water-cooled data center for dehumidification application using desiccant-coated heat exchangers, Energy Build. 346 (2025) 116196, https://doi.org/10.1016/j.enbuild.2025.116196.
[44] W. Guo, Z. Zhang, H. Wu, L. Ge, X. Liang, R. Mao, Experimental study on cooling and dehumidification performance of an ice storage air conditioner used in underground refuge chamber, Int. Commun. Heat Mass Tran. 146 (2023) 106930, https://doi.org/10.1016/j.icheatmasstransfer.2023.106930.
[45] Z. Han, Q. Ji, H. Wei, D. Xue, X. Sun, X. Zhang, X. Li, Simulation study on performance of data center air-conditioning system with novel evaporative condenser, Energy 210 (2020) 118521, https://doi.org/10.1016/j.energy.2020.118521.
[46] R.J. Moffat, Describing the uncertainties in experimental results, Exp. Therm. Fluid Sci. 1 (1988) 3–17, https://doi.org/10.1016/0894-1777(88)90043-X.
[47] B.-C. Du, Y.-L. He, Y. Qiu, Q. Liang, Y.-P. Zhou, Investigation on heat transfer characteristics of molten salt in a shell-and-tube heat exchanger, Int. Commun. Heat Mass Tran. 96 (2018) 61–68, https://doi.org/10.1016/j.icheatmasstransfer.2018.05.020.
[48] L. Miao, R. Wan, Z. Liu, H. Wu, Heat transfer simulation and performance optimization of plate-type phase change energy storage unit, Thermal Science Journal 28 (2024) 3865, https://doi.org/10.2298/TSCI230828107M.
[49] T.Ü. Erkek, M. Erkek, M.B. Aydın, K. Gezer, Experimental performance characterization of R-454B and R-410A in data center server rack mount cooling unit: energy efficiency and environmental impact assessment, Int. J. Refrig. 182 (2026) 469, https://doi.org/10.1016/j.ijrefrig.2025.12.007.
[50] X. Guo, H. Xu, L. Cao, B. Zhang, Innovative integration of mechanical refrigeration and loop thermosyphon with liquid reservoir control: enhancing energy efficiency and dynamic stability in data center cooling systems, Int. J. Refrig. 183 (2026) 112, https://doi.org/10.1016/j.ijrefrig.2025.11.019.
[51] P. Zhang, B. Wang, W. Wu, W. Shi, X. Li, Heat recovery from internet data centers for space heating based on an integrated air conditioner with thermosyphon, Renew. Energy 80 (2015) 396–406, https://doi.org/10.1016/j.renene.2015.02.032.
[52] A. Elbir, Dynamic phase change materials for sustainable energy storage: Long-term performance trends and enhancement strategies, J. Build. Eng. 113 (2025) 114030, https://doi.org/10.1016/j.jobe.2025.114030.
[53] A. Wadee, P. Walker, N. McCullen, V. Ferrandiz Mas, The effect of thermal cycling on the thermal and chemical stability of paraffin phase change materials (PCMs) composites, Mater. Struct. 58 (2024) 25, https://doi.org/10.1617/s11527-024-02556-y.
[54] C. Yang, Z. Li, S. Li, X. Cui, Q. Chen, Sustainable evaporative cooling driven by saline water sources: opportunities, challenges and solutions, Renew. Sustain. Energy Rev. 218 (2025) 115799, https://doi.org/10.1016/j.rser.2025.115799.
[55] H. Zhang, S. Shao, H. Xu, et al., Integrated system of mechanical refrigeration and thermosyphon for free cooling of data centers, Appl. Therm. Eng. 75 (2015) 185, https://doi.org/10.1016/j.applthermaleng.2014.09.060.